1 **Title:** Genetic variance in the murine defensin locus modulates glucose homeostasis

2 **Authors**: Stewart W.C. Masson[1,2,*], Rebecca C. Simpson[2,3,4], Harry B. Cutler[1,2],
3 Patrick W. Carlos[5,6], Oana C. Marian[2,7], Meg Potter[1,2], Søren Madsen[1,2], Kristen C.
4 Cooke[1,2], Niamh R. Craw[1,2], Oliver K. Fuller[1,2], Dylan J. Harney[1,2], Mark Larance[2,7],
5 Gregory J. Cooney[2], Grant Morahan[8], Erin R. Shanahan[1,2], Christopher Hodgkins[1,2],
6 Richard J. Payne[5,6], Jacqueline Stöckli[1,2], and David E. James[1,2,7,*]

7 *, corresponding authors: Stewart W.C. Masson (stewart.masson@sydney.edu.au),
8 David E. James (david.james@sydney.edu.au)

9 **Author affiliations:**

10 1. School of Life and Environmental Sciences, The University of Sydney, Sydney,
11 Australia
12 2. Charles Perkins Centre, The University of Sydney, Sydney, Australia
13 3. Melanoma Institute Australia, Sydney, Australia
14 4. Sydney Medical School, Faculty of Medicine and Health, The University of
15 Sydney, Sydney, Australia
16 5. School of Chemistry, The University of Sydney, Sydney, Australia
17 6. Australian Research Council Centre of Excellence for Innovations in Peptide
18 and Protein Science
19 7. School of Medical Sciences, The University of Sydney, Sydney, Australia
20 8. Centre for Diabetes Research, Harry Perkins Institute of Medical Research,
21 Murdoch, Australia

22 **Competing interests**: the authors declare no competing interests

Abstract

Insulin resistance is heritable; however, the underlying genetic drivers remain elusive. In seeking these, we performed genetic mapping of insulin sensitivity in 670 chow-fed Diversity Outbred in Australia (DOz) mice and identified a genome-wide significant quantitative trait loci (QTL) within the chromosome 8 defensin gene cluster. Defensins are antimicrobial peptides secreted from Paneth cells into the intestinal lumen that can alter the abundance of beneficial and detrimental microbes. Proteomic analysis of the small intestine from Diversity Outbred founder strains revealed that alpha-defensin 26 positively correlated with whole-body insulin sensitivity, and founder strain genetic contributions to the insulin sensitivity QTL. To validate these findings, we synthesised the secreted form of alpha-defensin 26 and performed diet supplementation experiments in two mouse strains with distinct endogenous alpha-defensin 26 expression levels. In validation of our DOz data, the strain with lower endogenous expression (C57BL/6J) exhibited improved insulin sensitivity and reduced gut permeability following defensin supplementation. In contrast, the higher expressing strain (A/J) exhibited hypoinsulinemia, glucose intolerance and muscle wasting. Gut microbiome profiling in these mice revealed both global and strain-specific changes including some observed in DOz mice positive for the putative insulin sensitivity allele. Inspired by previous work linking glucose homeostasis to gut microbiome mediated changes in plasma bile acids, we investigated these as a potential mechanism. As with metabolic changes, A/J but not C57BL/6J mice exhibited differential plasma bile acid concentrations following defensin supplementation. These data highlight the importance of considering individual differences when designing metabolic therapeutics and paves the way for further studies investigating links between the host genetics and the microbiome.

48 **Introduction**

49 Insulin resistance (IR) drives various pathologies including Type 2 Diabetes,
50 cardiovascular disease, various cancers, and some forms of neurological decline (1).
51 IR is characterised by a failure of peripheral tissues to respond to the hormone insulin
52 and decades of physiological and biochemical studies in mice and humans have
53 posited many underlying mechanisms. These include lipotoxicity (2, 3), reactive
54 oxygen species (4, 5), and inflammation (6, 7) among many others. On balance, these
55 potential mechanisms likely all drive IR to different extents across individuals, and no
56 one defect in insulin action is responsible for all pathology. This heterogeneity implies
57 a considerable genetic component and makes diagnosis and treatment at the
58 population level challenging. With some notable exceptions, genome-wide association
59 studies have struggled to identify loci for IR (8-10). One potential explanation is that
60 the diversity of human environments confounds genetic signals via complex gene-by-
61 environment interactions. Unfortunately, environmental factors are almost impossible
62 to control in humans.

63 Mice are a valuable tool for studying human diseases due to their genetic and
64 physiologic similarities. Moreover, they afford the precise environmental control
65 required to detect genetic loci associated with insulin resistance. Studies in panels of
66 inbred mouse strains fed different diets have begun to do this (11-15) and genetically
67 diverse mouse populations such as Jackson Labs' Diversity Outbred (DO) mice offer
68 promise thanks to their unparalleled genomic resolution (16-19). This can be
69 harnessed to map complex traits to genomic loci, inferring causality and informing
70 discovery of important mechanisms underlying insulin action. We have acquired a
71 similar population of mice, which we term Diversity Outbred in Australia (DOz). We

72 have used this population to investigate skeletal muscle insulin resistance (20) albeit
73 on a single diet, and studied the metabolic consequences of weight-cycling (21).
74 Further investigations in these models promise to uncover the genetic drivers of insulin
75 resistance, provide insight into complex gene-by-environment interactions, and
76 improve translatability from mice into humans (22).

77 Critically ‘environment’ also includes an individual's gut microbiome which is emerging
78 as a driver of host metabolic health with some taxa being beneficial and others
79 detrimental (23). Microbes can interact with the host both directly (24, 25) and via
80 diverse signalling molecules including metabolites (26, 27), peptides (28, 29), and bile
81 acids (30-33). Current research on the gut microbiome and insulin resistance often
82 focuses solely on these mechanisms in a feed-forward, microbe to host approach.
83 However, human genome-wide association and twin studies have revealed high levels
84 of genomic control over the microbiome (34, 35). In mice, a recent study revealed that
85 one quarter of all detected microbes have significant quantitative trait loci (QTL)
86 implying host regulation of their abundance (36). It is unknown whether genetic drivers
87 of microbial composition could also regulate IR via upregulating or downregulating
88 metabolically important microbes. Here we explore this notion using an unbiased
89 systems biology approach and ultimately identify an antimicrobial peptide as a
90 potential insulin sensitivity therapeutic with implications for personalised medicine.

Results

Whole body insulin sensitivity is genetically linked to the defensin locus on chromosome 8

To quantify whole body insulin sensitivity, we conducted glucose tolerance tests and insulin ELISAs on 670 chow fed male DOz mice (Figure 1A) and used these data to calculate the Matsuda Index (Figure 1B), a surrogate measure of insulin sensitivity (37). Consistent with our previous work (20), we observed striking variation in Matsuda Index despite all animals being housed under identical conditions and fed the same chow diet. We next performed genetic mapping of the Matsuda Index (Figure 1C) and identified 2 genome-wide significant quantitative trait loci (QTL), one on chromosome 2 at 162.2 Mbp and a second on chromosome 8 at 21.7 MBp. The chromosome 8 locus centred over the defensin gene cluster, a syntenic region shared between mice and humans (38), which contains 53 defensin genes and 22 defensin pseudogenes (Figure 1D). Considering previous links between defensins and metabolic disease (39-42) we selected this QTL for further validation.

Single nucleotide polymorphism (SNP) analysis of the defensin locus identified one intergenic SNP rs231642830, and one structural variant SV_8_21749161_21749163, with genome wide significant LOD scores (Figure 1E). We categorised mice by the number of minor alleles they carried at the rs231642830 SNP (AA = no minor alleles, AB = one copy, BB = two copies). Animals carrying the AB allele had identical glucose tolerance to ‘control’ AA mice despite a 50% reduction in insulin at the 15-minute time point (Figure 1F,G). These data suggest genetic variance at the defensin locus is linked to improved whole body insulin sensitivity.

Figure 1

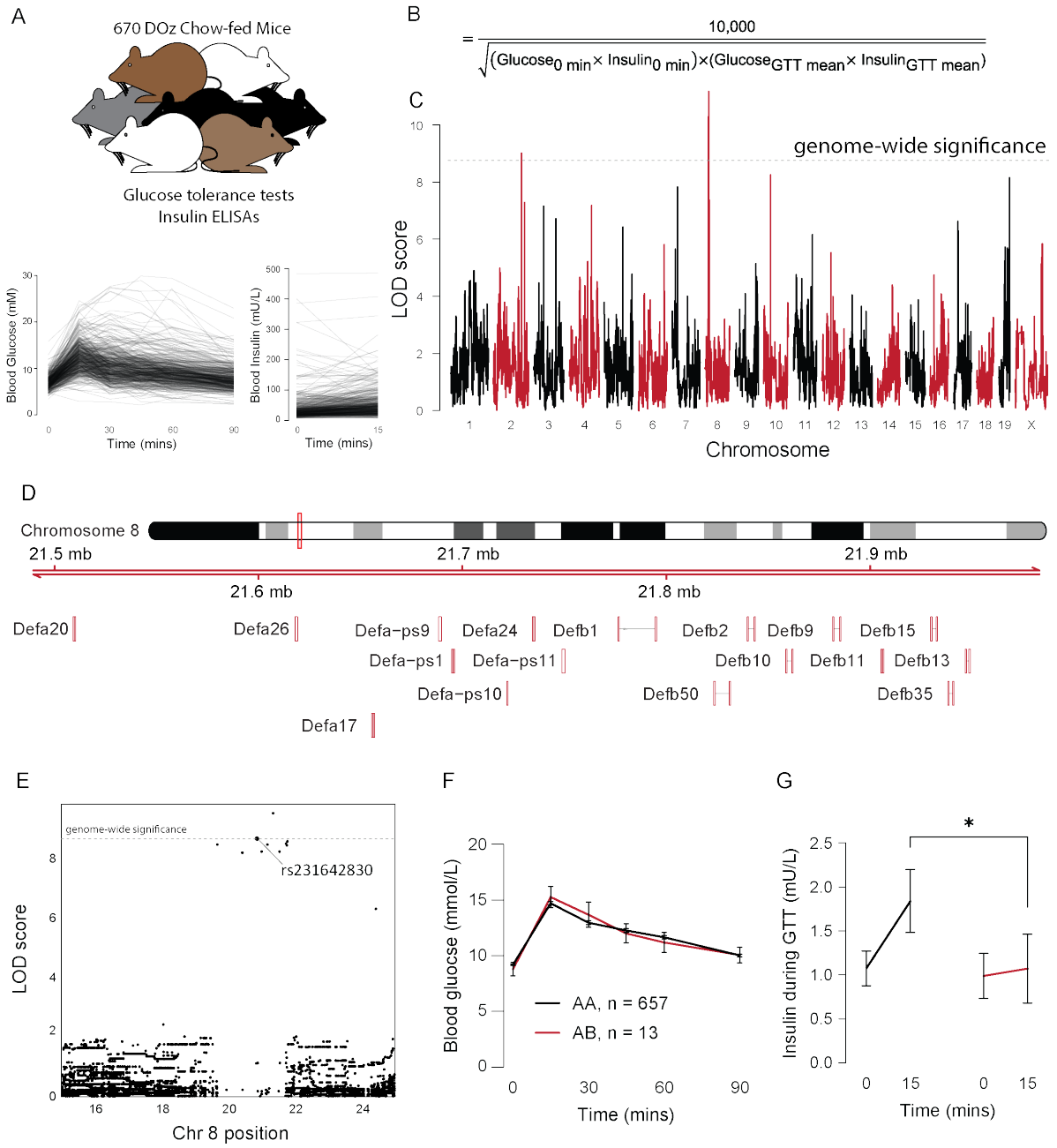

Figure 1 – Genetic mapping of insulin sensitivity in 670 chow-fed Diversity Outbred in Australia mice. A) Glucose and insulin concentrations during a glucose tolerance test in 670 DOz mice. **B)** The equation used to calculate the Matsuda Index from GTT data. **C)** Genetic mapping of the Matsuda Index in DOz mice. **D)** The defensin locus on chromosome 8. **E)** Single nucleotide polymorphism (SNP) mapping of the Matsuda Index on chromosome 8. **F)** Blood glucose concentrations during a glucose tolerance test of mice carrying the minor allele of rs231642830 and non-carrier controls. **G)** Blood insulin concentrations during a glucose tolerance test of mice carrying the minor allele of rs231642830 and

122 non-carrier controls. Data are mean with biological replicates are shown as individual data points or
123 noted in figure. **** P < 0.0001, *** P < 0.001, ** P < 0.01, * P < 0.05.

124

125 *A single nucleotide polymorphism within the defensin locus associates with insulin*
126 *sensitivity and increased Akkermansia muciniphila abundance*

127 Defensins are an ancient component of the immune system, found across the tree-of-
128 life from plants to humans. They are small peptides (29-40 amino acids) with potent
129 antibacterial and antiviral activities (43). In mice, defensins are secreted from Paneth
130 cells in the intestinal crypt into the gut lumen to modulate microbial composition (Figure
131 2A). Therefore, we performed 16S rRNA gene amplicon sequencing to profile the
132 microbiome composition of mice from three groups: 1) mice carrying the putative
133 protective rs231642830 allele (AB), 2) cage mates of these mice, and 3) a subset of
134 AA control mice (Figure 2B). Because mice are coprophagic, analysing cage mates
135 allows us to test for co-housing effect on insulin sensitivity, which could indicate a
136 microbiome mediated mechanism of action.

137 All AB mice had been separately housed, and AA control mice were chosen at random
138 from across 7 different cages. No significant difference in alpha diversity (Inverse
139 Simpson; a measure of ecological diversity within a group) was observed between
140 groups (Figure 2C). However beta-diversity analysis (Bray-Curtis dissimilarity and
141 PERMANOVA; a measure of ecological diversity between group) (Figure 2D) of our
142 three groups revealed a trend towards differences in overall microbiome composition
143 between AB mice and AA controls (p value = 0.05), and between AA controls and cage
144 mates of AB mice (p value = 0.055), but not between AB mice and their cage mates
145 (p value = 0.622). However, analysis of the pooled microbiomes (AB mice + cage
146 mates), against the AA control mice revealed distinct microbiomes (p value = 0.009).

147 This is consistent with mice carrying the minor allele possessing altered microbiomes,
148 and this being transmitted to their cage mates.

149 Differential abundance analysis of these groups by Analysis of Compositions of
150 Microbiomes with Bias Correction (ANCOM-BC) revealed that compared to AA
151 controls, *Akkermansia muciniphila* (Figure 2E, F), *Bifidobacterium pseudolongum*
152 (Figure 2E, G) and *Ligilactobacillus spp.* (Figure 2G, H), were higher in cage mate and
153 AB mice, while *Limosilactobacilius spp*. (Figure 2H, I) were lower. Among these
154 strains, *Akkermansia muciniphila* stands out as it has strong links to metabolic health
155 and has been shown to increase in response to α-defensin administration in C57BL6/J
156 mice (28, 29, 42, 44, 45). Critically we observed the same overall relationship for
157 insulin sensitivity Matsuda Index higher in AB mice, and trended higher in cage mates
158 relative to AA control mice. This suggests that insulin sensitivity differences between
159 AA and AB mice may be transferable by cohousing.

Figure 2

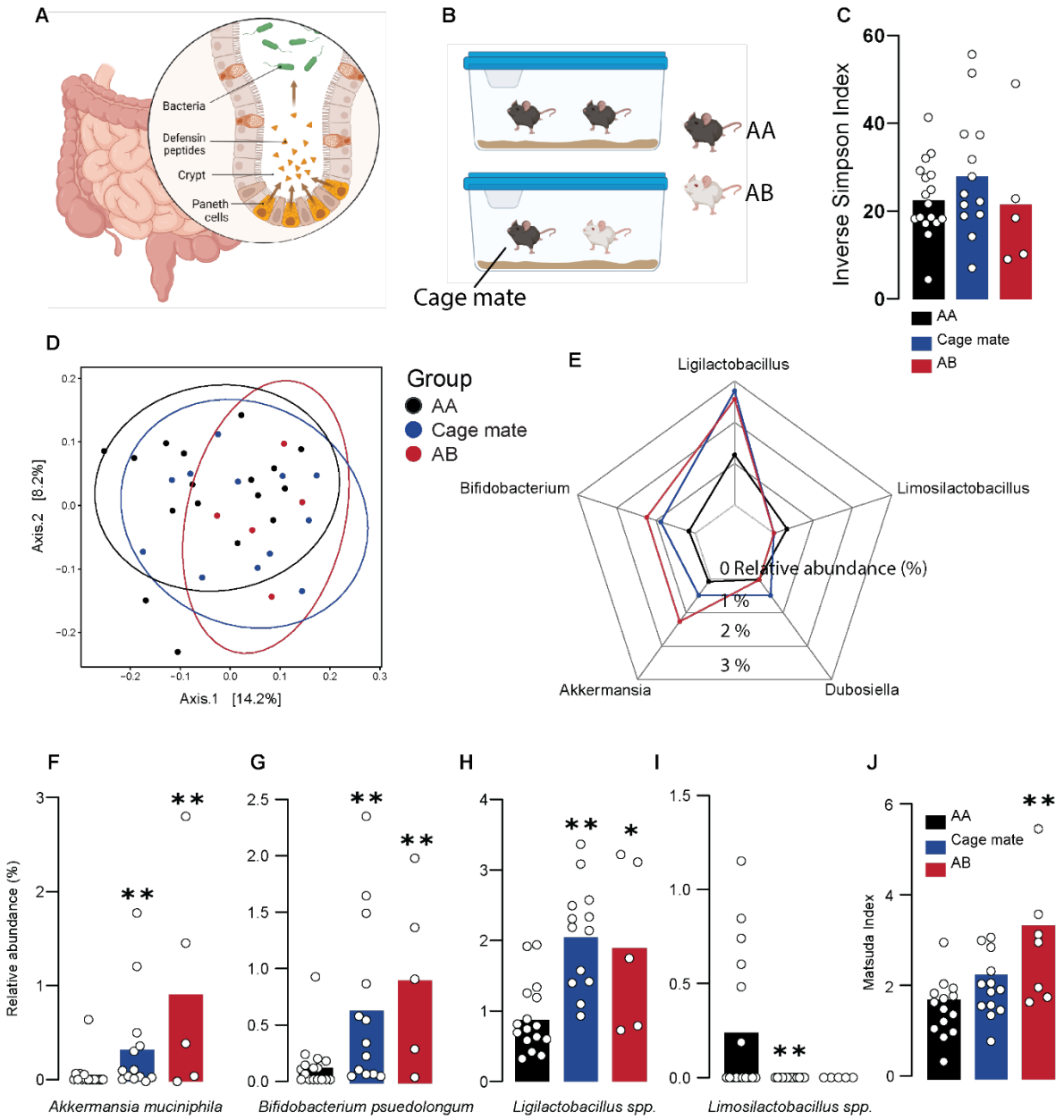

Figure 2 – Analysis of microbial composition and co-housing effects in mice carrying a putative insulin sensivity allele within the defensin locus. A) Schematic of murine defensin secretion from Paneth cells into the small intestine. **B)** Schematic of the study design including mice carrying rs231642830 (AB), non-carrier controls (AA), and the cage mates of mice carrying rs231642830 (Cage mate). **C)** Alpha diversity (Inverse Simpson) of AB, AA and Cage mates. **D)** Visualisation of beta-diversity between AB, AA and Cage mate mice calculated by Bray-Curtis dissimilarity. **E)** Relative abundances of differential represented microbes between AB, AA and Cage mate mice. **F)** Relative abundance of *Akkermansia muciniphila* in AB, AA and Cage mate mice. **G)** Relative abundance of

169 *Bifidobacterium psuedolongum* in AB, AA and Cage mate mice. **H)** Relative abundance of
170 *Ligilactobacillus spp*. in AB, AA and Cage mate mice. **I)** Relative abundance of *Limosilactobacillus spp*.
171 in AB, AA and Cage mate mice. **J)** Matsuda Index in AB, AA and Cage mate mice. Data are mean with
172 biological replicates are shown as individual data points or noted in figure. **** P < 0.0001, *** P <
173 0.001, ** P < 0.01, * P < 0.05.

174

175 *Alpha defensin 26 positively correlates with insulin sensitivity and founder strain*
176 *contributions towards the Matsuda QTL in the defensin locus.*
177 We next sought to identify the specific defensin isoform that confers variation in insulin
178 sensitivity by performing proteomic analysis of small intestines from a subset of
179 Diversity Outbred founder strains (Figure 3A). Since the genomes of these strains
180 have been fully sequenced (16) we are able to validate experiments in DOz with data
181 generated in the founder strains via estimates the of founder contributions at the Chr
182 8 locus.

183 Consistent with our previous work (11) and that of others (14, 15) we observed
184 significant variation in glucose tolerance (Figure S1A-H), insulin sensitivity, and
185 adiposity between inbred founder strains (Figure 3BC). Proteomic analysis of small
186 intestinal tissue from these animals identified a total of 5,529 proteins with 4,822
187 proteins, including 9 defensin isoforms, found in at least 50% of samples. To rule out
188 strain level differences in Paneth cell abundance (46) influencing the apparent
189 defensin expression levels, we normalised defensin peptide expression to the average
190 of all defensins within each strain. Correlation analysis of mean normalised defensin
191 isoform expression revealed that a single isoform, alpha-defensin 26 (Defa26), was
192 positively correlated with insulin sensitivity ($R = 0.73$, $P < 0.05$; Figure 3D,E). We then
193 calculated the QTL founder effects for the chromosome 8 locus. Among the founder

194 strains, A/J, NOD/ShiLtJ, and to a lesser extent 129S1/SvlmJ, contributed positively
195 while CAST/EiJ, NZO/HILtJ, WSB/EiJ, C57BL/6J and PWK/PhJ contributed negatively
196 (Figure 3F). Correlating the founder effects at 21.7 MBp on chromosome 8 with mean
197 normalised defensin levels revealed that only alpha-defensin 26 levels varied in
198 accordance with the contributions of each founder strain to the QTL (R = 0.89, P <
199 0.01; Figure 3G).

Figure 3

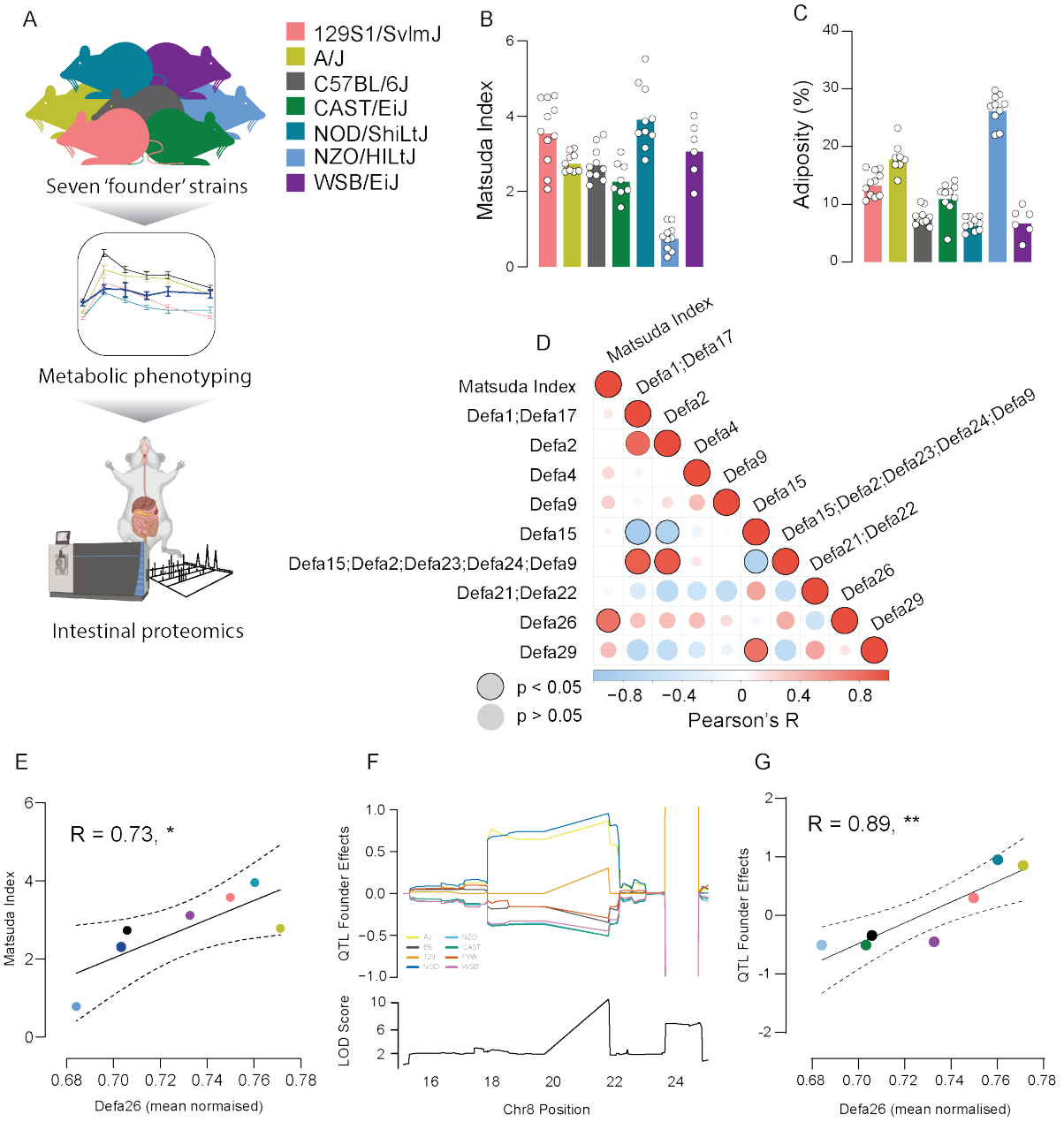

200

201 **Figure 3 – Proteomic analysis of small intestinal tissues from Diversity Outbred founder strains.**
202 **A)** Schematic of study design to investigate insulin sensitivity and defensin protein expression in small
203 intestines of inbred mouse strains. **B)** Matsuda Index in Diversity Outbred founder strains. **C)** Adiposity
204 in Diversity Outbred founder strains. **D)** Correlations of all quantified defensin peptides (Defa) with
205 Matsuda Index across Diversity Outbred founder strains. **E)** Correlation of mean normalised alpha-
206 defensin 26 abundance with Matsuda Index in Diversity Outbred founder strains. **F)** founder strain
207 contribution estimates for the DOz Matsuda Index QTL on chromosome eight. **G)** Correlation of founder
208 strain contribution estimates for the DOz Matsuda Index QTL with mean normalised alpha-defensin 26
209 abundance. Dashed lines denote 95% confidence intervals. Data are mean with biological replicates
210 are shown as individual data points or noted in figure. **** $P < 0.0001$, *** $P < 0.001$, ** $P < 0.01$, * $P <$
211 0.05

212

213 *Dietary supplementation with alpha-defensin 26 has strain specific effects on*
214 *metabolism and body composition*

215 Genetic mapping in DOz mice and proteomics in the founder strains suggested that
216 alpha-defensin 26 is a positive regulator of insulin sensitivity. To experimental test this
217 we synthesised the luminal (to mimic post-processing secretion) form of alpha-
218 defensin 26 by 9-fluorenylmethyloxycarbonyl-solid-phase peptide synthesis (Fmoc-
219 SPPS), followed by folding (47). We also synthesised the luminal form of human alpha-
220 defensin 5 as a positive control since this peptide has previously been shown to
221 improve glucoregulatory control in C57BL/6J mice (42).

222 To first validate Fmoc-SPPS as a method to produce metabolically beneficially
223 peptides we fed C57BL/6J mice with either a high-fat high-sugar western-style diet
224 (WD) or a WD supplemented with 10 ng/g of human alpha-defensin 5 for eight weeks.
225 Consistent with previous work (42), mice fed a WD supplemented with chemically
226 synthesised alpha defensin 5 had attenuated weight gain and reduced adiposity but

227 normal lean mass (Figure S2A-C) when compared to control mice fed a control WD.
228 Alpha-defensin 5 supplementation also improved insulin sensitivity, evidenced by
229 equivalent glucose tolerance but lower insulin levels relative to control mice (Figure
230 S2D, E). These results indicate that chemically synthesised alpha-defensin peptides
231 behave comparably to previous peptides generated by traditional expression systems
232 (39, 40, 42). Based on these results we proceeded with alpha-defensin 26
233 supplementation (Def26).

234 We hypothesised that in strains with low alpha-defensin 26 expression, diet
235 supplementation would be protective while in strains with relatively higher abundance,
236 supplementation would have no effect. To this end, we selected the metabolic disease
237 susceptible C57BL/6J (low abundance of alpha-defensin 26) and the metabolic
238 disease resistant A/J (high abundance of alpha-defensin 26) and repeated the above
239 study feeding both strains with either WD or WD + Def26. After 8 weeks of diet and
240 supplement intervention, we observed no differences in body weight in either strain
241 relative to WD fed control mice (Figure 4A, B), however, C57BL/6J mice gained less
242 adiposity (Figure 4C). Strikingly, A/J but not C57BL/6J mice fed WD + Def26 lost
243 approximately 1 gram of skeletal muscle mass (Figure 4D, Figure S3A-C). Def26
244 supplementation did not affect food intake in either strain (Figure 4E).

245 To assess potential effects on of alpha-defensin 26 supplementation on gut health we
246 measured gut permeability *in vivo* by assessing FITC-Dextran translocation into the
247 blood following oral administration, and by measuring the overall length of the small
248 intestine (24, 48). Def26 supplementation lowered gut permeability in both strains,
249 however, this was only significant in C57BL/6J mice (Figure S3D). Neither strain
250 exhibited differences in small intestinal length (Figure S3E).

251 Alpha-defensin 26 supplementation did not alter glucose tolerance of C57Bl6/J mice
252 and in contrast to our prediction, it led to impaired glucose tolerance in A/J mice (Figure
253 4F-H). Despite no apparent effect on glucose tolerance, C57Bl6/J mice fed a WD +
254 Def26 diet had lower blood insulin levels during the GTT suggesting an improvement
255 in insulin sensitivity (Figure 4I), consistent with observations in AB DOz mice. In A/J
256 mice, as well as triggering relative glucose intolerance, alpha-defensin 26
257 supplementation induced significant fasting hypoinsulinemia and completely abolished
258 the glucose induced increase in blood insulin levels, suggesting an impairment in
259 insulin secretion (Figure 4J).

Figure 4

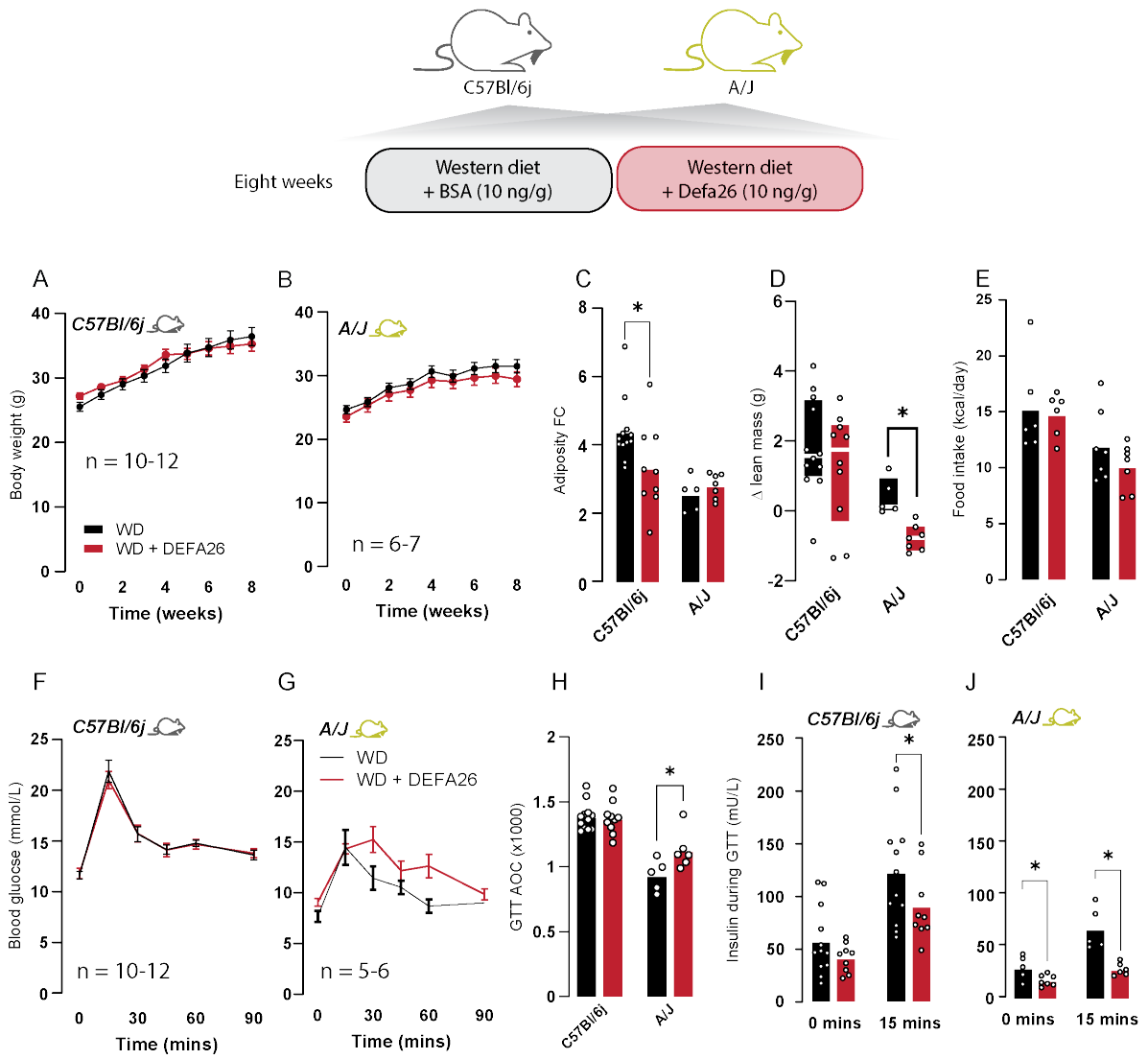

260

261 **Figure 4 – Effect of alpha-defensin 26 supplementation on insulin sensitivity and body**
262 **composition in western-diet fed C57BL/6J and A/J mice. A)** Body weight of C57BL/6J mice fed
263 either a WD or a WD + Def26. **B)** Body weight of A/J mice fed either a WD or a WD + Def26. **C)** Fold-
264 change in adiposity in mice fed either a WD or a WD + Def26. **D)** Change in lean mass in mice fed
265 either a WD or a WD + Def26. **E)** Food intake in mice fed either a WD or a WD + Def26. **F)** Blood
266 glucose concentrations during a glucose tolerance test in C57BL/6J mice fed either a WD or a WD +
267 Def26. **G)** Blood glucose concentrations during a glucose tolerance test in A/J mice fed either a WD or
268 WD + Def26. **H)** Area-of-the-curve (AOC) for glucose during a glucose tolerance test in mice fed either
269 a WD or a WD + Def26. **I)** Blood insulin concentrations during a glucose tolerance test in C57BL/6J
270 mice fed either a WD or a WD + Def26. **J)** Blood insulin concentrations during a glucose tolerance test
271 in A/J mice fed either a WD or a WD + Def26. Data are mean with biological replicates are shown as
272 individual data points or noted in figure. **** $P < 0.0001$, *** $P < 0.001$, ** $P < 0.01$, * $P < 0.05$

273

274 *Alpha-defensin supplementation induces strain specific effects on the microbiome.*
275 The defensin locus appears to be genetically linked to with insulin sensitivity via the
276 growth of certain metabolically beneficial microbes. To validate these findings, we
277 performed 16S rRNA amplicon sequencing and ANCOM-BC on caecal contents from
278 WD and WD + Def26 fed mice. Encouragingly, and consistent with results in AB DOz
279 mice (Figure 2F, I), *Akkermansia muciniphila* was enriched in both C57BL/6J and A/J
280 strains fed WD + Def26 (Figure 5A,B), while *Limosilactobacillus spp* was depleted in
281 WD + Def26 fed C57BL/6J mice relative to WD controls (Figure 5A). In addition,
282 *Alloprevotella spp* (Figure 5A,B) was enriched in both strains, and although not
283 differentially abundant in AA or AB DOz mice, has been previously linked to defensin
284 supplementation (44).

285 Overall, alpha-diversity was higher in A/J mice, and this was lowered by defensin 26
286 supplementation suggesting a potentially detrimental effect on microbial ecological

287 diversity in this strain (Figure S4A). Beta-diversity analysis revealed divergent
288 microbiomes between C57Bl6/J and A/J mice, as well as differences between those
289 mice fed a WD and WD + Def26 (Figure S4B) suggesting Def26 supplementation does
290 alter the gut microbiome. At the Order level, *Bacilli* and *Bacteroidia* were differentially
291 abundant between C57BL/6J and A/J mice with the former being higher in C57BL/6J
292 and the latter being higher in A/J mice (Figure S4C-G). Supplementation with alpha-
293 defensin 26 decreased *Clostridia* only in A/J mice (Figure S4A). At the species level,
294 ANCOM-BC revealed comparable numbers of differentially abundant taxa between
295 diets in C57BL/6J and A/J mice (Figure 5C). However, the nature of these differences
296 was relatively strain specific, and only three differential abundant taxa were shared
297 between strains (Figure 5A,B). These include the aforementioned *Akkermansia*
298 *muciniphila* (Figure 5D) and *Alloprevotella spp* (Figure 5E), as well as a third microbe
299 *Erysipelatoclostridium spp* (Figure 5F). Highlighting strain specific alterations in
300 microbial abundance, *Erysipelatoclostridium spp*. was enriched by defensin
301 supplementation in C57BL/6J mice but depleted in A/J mice.

302

Figure 5

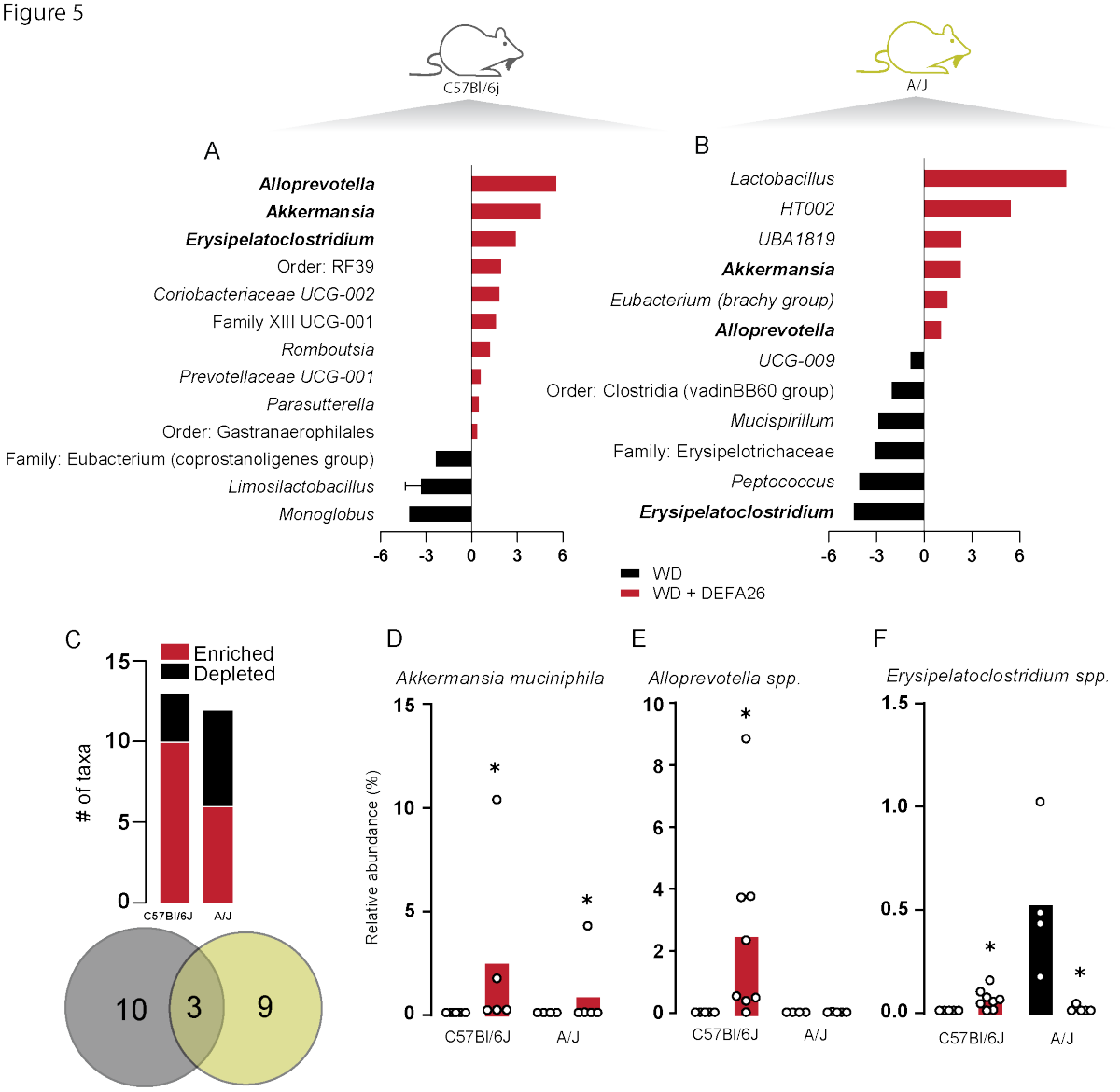

Figure 5 – Validation of alpha-defensin 26 effects on gut microbial composition in C57BL/6J and A/J mice. A) Differentially abundant microbes in C57BL/6J mice fed either a WD or a WD + Def26. **B)** Differentially abundant microbes in A/J mice fed either a WD or a WD + Def26. **C)** Comparison of differentially abundant microbial taxa in mice fed either a WD or a WD + Def26 assessed by ANCOM-BC. **D)** *Akkermansia muciniphila* relative abundance in C57BL/6J and A/J mice fed either a WD or a WD + Def26. **E)** *Alloprevotella spp.* relative abundance in C57BL/6J and A/J mice fed either a WD or a WD + Def26. **F)** *Erysipelatoclostridium spp.* relative abundance in C57BL/6J and A/J mice fed either a WD or a WD + Def26. Bold text denotes overlap between C57BL/6J and A/J. Data are mean with biological replicates are shown as individual data points or noted in figure. **** $P < 0.0001$, *** $P < 0.001$, ** $P < 0.01$, * $P < 0.05$

314

315 *Changes in circulating bile acids may explain global and strain specific effects of*
316 *alpha-defensin 26 on metabolism*

317 Improved insulin sensitivity and increased relative abundances of the same microbes
318 enriched in mice carrying the putative DOz insulin sensitivity allele following Def26
319 supplementation (Figure 2E, 5A, B), broadly validates a microbiome-mediated genetic
320 link between defensin peptides and insulin sensitivity. However, a number of questions
321 remain. Firstly, by what mechanism do defensin mediated microbial changes influence
322 host metabolism? Secondly, although *Akkermansia muciniphila* serves as a
323 convenient positive control, microbes rarely act in isolation to influence host
324 metabolism. Therefore, what other microbial changes mediate the effect of defensin
325 supplementation on host metabolism?

326 In an attempt to answer these questions and interrogate our data further we correlated
327 the relative abundances of all microbial genera with insulin sensitivity (Matsuda Index),
328 insulin levels during a GTT (0 and 15 minutes), and changes in body composition (lean
329 mass and adiposity). Of our 87 quantified microbial genera, 35% significantly
330 correlated with at least one metabolic phenotype (Figure 6A). In some instances, the
331 correlations between microbial taxa and metabolic phenotypes were stronger than
332 those between two well characterised metabolic characteristics. For example,
333 *Lachnoclostridium spp.* positively correlated with fasting insulin levels (Figure S4K; R
334 = 0.83, p-value < 0.0001) more strongly than fasting insulin correlated with changes in
335 adiposity (R = 0.6696, p-value = 0.002).

336 Microbes influence metabolism via a plethora of modalities, one of the most potent
337 being secondary bile acids. Specifically, gut microbiome derived bile acids have been

338 linked to insulin secretion and lean mass (31, 49, 50), two of the key phenotypic
339 changes observed in C57BL/6J and A/J mice supplemented with alpha-defensin 26.
340 Specifically microbial transplant from CAST/EiJ mice into C57BL/6J mice altered
341 plasma bile acids and completely abolished glucose-stimulated insulin secretion (31).
342 Inspired by this work, we set out to assess whether defensin mediated editing of the
343 microbiome could be driving phenotypic changes via circulating bile acids.

344 Using liquid chromatography-mass spectrometry (LC-MS) we measured the
345 abundance of 16 primary and secondary bile acids in plasma from a subset of
346 C57BL6/J and A/J mice fed either a WD or WD + Def26 (Figure S5A, B). Consistent
347 with greater observed effects on glucose homeostasis and body composition, principal
348 component analysis of these data revealed that A/J but not C57BL/6J mice clustered
349 in groups based on diet (Figure 6B). To ascertain a potential path of causality from
350 microbes to observed phenotypes we integrated plasma bile acid data with
351 phenotypically important microbes (those with significant associations with metabolic
352 phenotypes; Figure 6A) by correlation and hierarchical clustering (Figure S5C).

353 These relationships can be visualised in a hive plot (51), which links nodes (in this
354 case microbe relative abundances, bile acid concentrations and phenotypic traits) via
355 lines coloured by correlation strength and direction (Figure 6C). Although 31 microbes
356 were associated with metabolic phenotypes, only 4 were also strongly correlated with
357 plasma bile acid concentrations: Family: Muribaculaceae, *Lachnoclostridium spp,*
358 *Faecalibaculum spp,* and *Monoglobus spp.* Tracing their relationships to metabolic
359 phenotypes via bile acids revealed 4 potentially important candidates: the composite
360 measure of tauro-ursodeoxycholic acid and tauro-hyodeoxycholic acid (TUDCA +
361 THDCA), alpha-Muricholic acid (αMCA), Tauro-chenodeoxycholic acid (TCDCA), and
362 Tauro-lithocholic acid (TLCA). In turn these 4 bile acids correlate with a subset of

363 metabolic phenotypes, insulin levels (both fasting and during a GTT) adiposity fold-
364 change as well as the Matsuda Index.

365 Visualising these data in this way reveals a number of intriguing relationships. For
366 example, *Lachnoclostridium spp* positively correlates with fasting insulin levels and
367 adiposity fold-change (Figure 5D), also positive correlates with TUDCA + THDCA and
368 αMCA (Figure 6E). These bile acids in turn associate with different metabolic
369 phenotypes. TUDCA + THDCA positively correlates with fasting insulin levels but not
370 adiposity fold-change (Figure 6E). The opposite is true for αMCA, which correlates
371 with adiposity fold-change but not fasting insulin levels (Figure 6E). These data
372 suggest that *Lachnoclostrdium* may modulate host metabolism and body composition
373 via distinct bile acid mediated mechanisms.

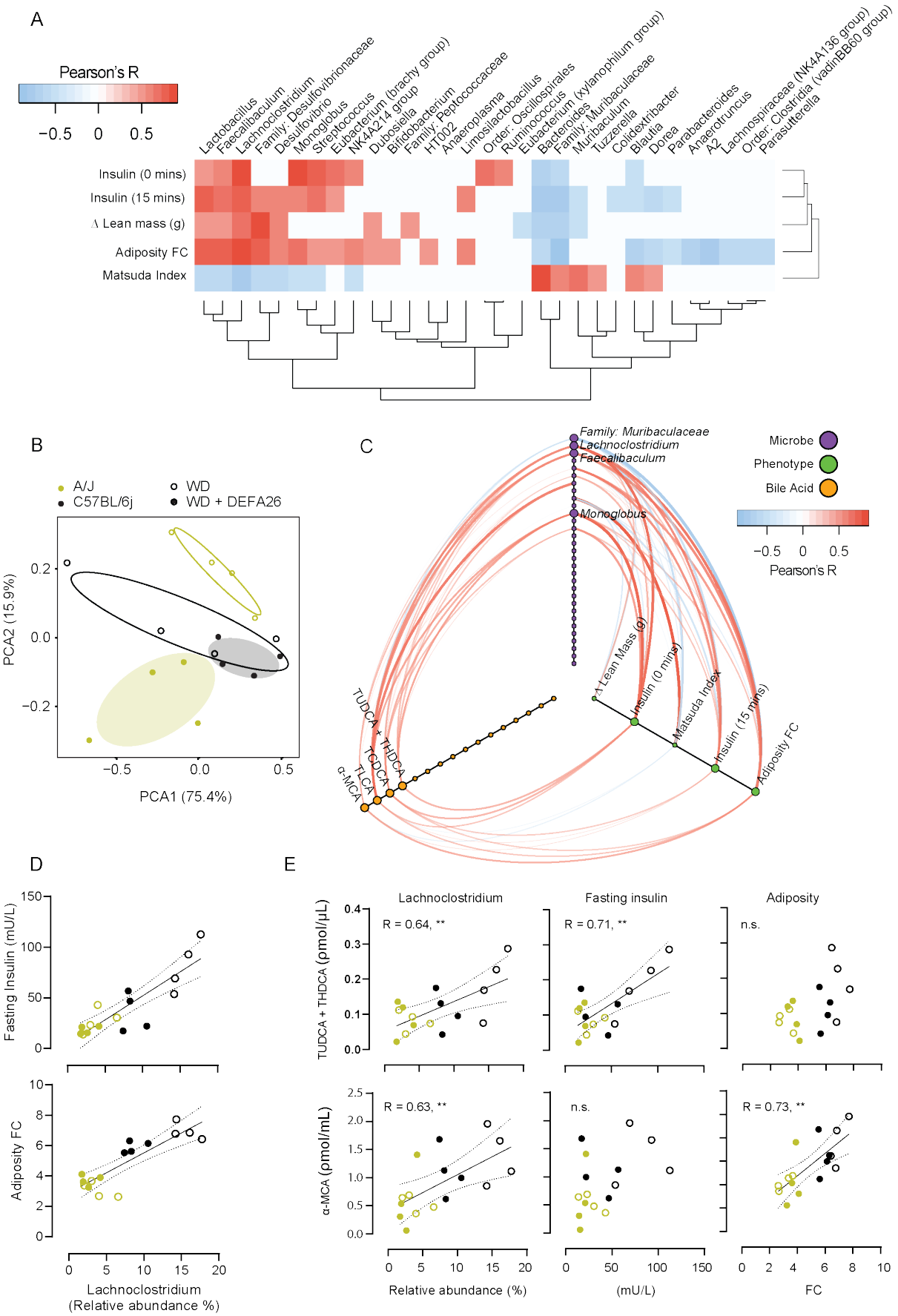

374

375 **Figure 6 – Integrative analysis of plasma bile acid concentrations and gut microbial abundance**

376 **in C57BL6/J and A/J mice. A)** Heatmap representation of significant correlations between metabolic
377 phenotypes and relative abundances of microbial genera. **B)** Principal component analysis of plasma
378 bile acid concentrations in C57BL/6J and A/J mice fed either a WD or a WD + Def26. **C)** Hive plot
379 representation of relationships between microbial genera which associate with metabolic phenotypes
380 and plasma bile acid concentrations. Node colour denotes feature class (Phenotype, Microbe, Bile Acid)
381 while width and colour of line denotes strength of correlation. **D)** Correlation of fasting insulin levels and
382 adiposity fold-change with *Lachnoclostridium spp*. relative abundance in in C57BL/6J and A/J mice fed
383 either a WD or a WD + Def26. **E)** Correlations of TUDCA + THDCA and α-MCA with *Lachnoclostridium*
384 *spp.*, fasting insulin and adiposity fold-change in C57BL/6J and A/J mice fed either a WD or a WD +
385 Def26. Dashed lines indicate 95% confidence intervals. Data are mean with biological replicates are
386 shown as individual data points or noted in figure. **** $P < 0.0001$, *** $P < 0.001$, ** $P < 0.01$, * $P < 0.05$

387

388 **Discussion**

389 Dysbiosis is a well-documented feature of the metabolic syndrome (52, 53), and
390 restoring normal microbiome function has been touted as a potential therapeutic for
391 insulin resistance (27, 54). Here we provide the first evidence that genetic variation in
392 the defensin locus can have meaningful impacts on host metabolic health. This is
393 consistent with previous studies in C57BL6/J mice showing that defensins can
394 promote a metabolically beneficial microbiome (39, 42, 44), In humans, Defa26 is
395 orthologous to DEFA3 and DEFA6 (55). Searching of the Type 2 Diabetes Knowledge
396 (56) portal reveals a significant association between the intronic SNP rs1005910425
397 in DEFA6 with insulin sensitivity (BMI-adjusted fasting insulin). Whether this SNP
398 associates with differential abundance of metabolically beneficial microbial taxa or
399 defensin peptides is unclear but is an exciting avenue of future inquiry. Our data also
400 highlights the importance of individual genomic and phenotypic variation when
401 considering the development of treatment strategies as illustrated by improved insulin

402 sensitivity in C57BL6/J mice but muscle wasting and glucose intolerance in A/J mice
403 (Figure 4 and S3).

404 In our study, *Akkermansia muciniphila* served as an encouraging positive control for
405 the effect of defensin supplementation on the microbiome. However, it also has well
406 characterised effects on glucose metabolism and insulin resistance via GLP1
407 secretion and improved gut integrity (28, 29). Along with muscle wasting observed in
408 A/J mice, a well-documented effect of GLP1-based therapies (57, 58) in humans, we
409 considered upregulated GLP1 as a potential mechanism. However, this seems
410 unlikely as GLP1 is an incretin hormone, but both A/J and C57BL/6J mice exhibit lower
411 levels of circulating insulin. This ultimately prompted us to investigate alternative
412 mechanisms beyond *Akkermansia muciniphila*, arriving upon bile acid metabolism.
413 Bile acids are secreted into the intestinal lumen where they aid in lipid absorption (59),
414 while in the gut they can also be modified by various microbes before being
415 reabsorbed and returned to the liver via the enterohepatic circulation (59). A small
416 percentage of these microbially modified reabsorbed bile acids escape into the
417 peripheral circulation and act upon tissues through the G protein-coupled bile acid
418 receptor 1 (TGR5) and farnesoid X receptor (FXR) (49, 60, 61).

419 Consistent with a more striking metabolic phenotype, circulating bile acids were most
420 substantially altered by defensin supplementation in A/J mice. To interrogate this data
421 further we correlated circulating bile acid concentrations with gut microbial
422 abundances and metabolic phenotypes across both strains. This identified several
423 potential pathways from a community of microbes to 4 plasma bile acid species
424 (TUDCA + THDCA, TCDCA, TLCA, and α-MCA). Notably, TCDCA has been linked to
425 glucose homeostasis via well characterised effects on insulin secretion and
426 transcription (50, 62). Our network also suggested a role for αMCA in the regulation of

427 adiposity. This is a previously undocumented link, however mice with adipocyte
428 specific deletion of FXR exhibit adipocyte hypertrophy and downregulated lipolysis
429 (63), consistent with FXR-mediated expression of key lipolytic enzymes *Atgl* and *Hsl*
430 (64). Considering αMCA is a FXR antagonist (65), increased plasma concentrations,
431 perhaps related to gut microbial composition, may be inhibiting adipocyte lipolysis
432 leading to increased relative diet-induced weight gain even in the absence of lipolysis
433 inhibiting insulin.

434 Interestingly, the loss of lean mass in A/J mice fed alpha-defensin 26, arguably the
435 most striking metabolic phenotype generated by alpha-defensin feeding, appears to
436 be bile acid independent. In our network, no single bile acid that was quantified was
437 associated with lean mass, despite strong associations between bile acids and other
438 phenotypes linked to lean mass changes, such as insulin sensitivity. This suggests
439 that changes in lean mass are either modulated by bile acids indirectly via hormones
440 such as insulin or FGF15 (49, 66, 67), or by bile acid independent mechanisms. Both
441 are possible as insulin also regulates cellular growth both directly and via the
442 glucagon-insulin axis (68-70). Suppression of insulin levels will cause glucagon levels
443 to increase (71, 72), driving muscle wasting. Conversely, microbial derived short-chain
444 fatty acids such as acetate have previously been linked to muscle mass and function
445 independently of bile acids (73-75).

446 A key question raised by our data is why A/J mice respond differently to C57BL/6J
447 mice when supplemented with alpha-defensin 26. C57BL/6J mice exhibit greater
448 insulin sensitivity and reduced adiposity, consistent with our hypothesis and previous
449 studies using defensin-based metabolic therapeutics (39, 41, 42, 44). In contrast, A/J
450 mice exhibit hypoinsulinemia, muscle wasting and glucose intolerance. These
451 differences may reflect higher endogenous alpha-defensin 26 in A/J mice. In

452 C57BL/6J, 10 ng/g of alpha-defensin 26 may modestly alter the microbiome, improving
453 gut integrity and insulin sensitivity without disrupting bile acid metabolism. Conversely
454 in A/J mice the same dose may combine with higher baseline expression to create an
455 environment which is now toxic to certain microbial species, disrupting bile acid
456 metabolism, abolishing bile acid signalling in the pancreas leading to fasting
457 hypoinsulinemia, muscle wasting and glucose intolerance. An alternative mechanism
458 explaining strain specific responses to alpha-defensin supplementation centres
459 around baseline differences in microbiome composition. Indeed, other studies
460 including comparison of A/J and C57BL/6J microbiomes (76-78) have shown that the
461 baseline microbiome significantly alters the response to microbiome targeting
462 therapeutics. In our study, delineating this effect from genomic differences between
463 strains is challenging but requires further investigation, potentially via lower doses of
464 alpha-defensin 26 in A/J mice or homogenisation of microbiomes before
465 supplementation. Whatever the driver of these differences, it is clear that individual
466 variation must be considered when designing metabolic disease therapeutics.

467 While many of the genetic drivers of insulin sensitivity remain elusive, here we uncover
468 one potential link via defensin peptides and the gut microbiome. Curiously, if we
469 consider the microbiome as part of an individual's environment, our data suggest a
470 complex form of gene-by-environment interaction. Rather than be acted upon by the
471 environmental component i.e. diet, genetic variants within the defensin locus are
472 acting upon the environment to produce heterogenous metabolic outcomes.

473 **Methods**

474 *Mouse breeding and phenotyping*

475 Male 'Diversity Outbred from Oz' (DOz) mice were bred and housed at the Charles
476 Perkins Centre, University of Sydney, NSW, Australia as previously described (20).
477 The DOz mice used in this study were outbred for 27 to 36 generations and comprised
478 a total of 670 male DOz mice across 9 separate cohorts. Genomic DNA was isolated
479 from each mouse and subjected to SNP genotyping (79), followed by genotyping
480 diagnostics and cleaning as described (80). Experiments were performed in
481 accordance with NHMRC guidelines and under approval of The University of Sydney
482 Animal Ethics Committee, approval numbers #1274 and #1988. To delineate genetic
483 from cage-effects, mice were randomised into cages of 3-5 at weaning. All mice were
484 maintained at 23°C on a 12-hour light/dark cycle (0600-1800) and given *ad libitum*
485 access to a standard laboratory chow diet containing 16% calories from fat, 61%
486 calories from carbohydrates, and 23 % calories from protein or a high-fat high-sugar
487 diet (western diet; WD) containing 45% calories from fat, 36% calories from
488 carbohydrate and 19% calories from protein (3.5%g cellulose, 4.5%g bran, 13%g
489 cornstarch, 21%g sucrose, 16.5%g casein, 3.4%g gelatine, 2.6%g safflower oil,
490 18.6%g lard, 1.2%g AIN-93 vitamin mix (MP Biomedicals), 4.95%g AIN-93 mineral mix
491 (MP Biomedicals), 0.36%g choline and 0.3%g L-cysteine). Fat and lean mass
492 measures were acquired via EchoMRI-900 (EchoMRI Corporation Pte Ltd, Singapore)
493 at 14 weeks of age. Glucose tolerance was determined by oral glucose tolerance test
494 (GTT) at 14-weeks of age by fasting mice for 6-hours (0700-1300 hrs) before oral
495 gavage of 20% glucose solution in water at 2 mg/kg lean mass. Blood glucose
496 concentrations were measured directly by handheld glucometer (Accu-Chek, Roche
497 Diabetes Care, NSW, Australia) from tail blood 0, 15, 30, 45, 60, 90 minutes after oral

498 gavage of glucose. Blood insulin levels at the 0- and 15-minute time points were
499 measured by mouse insulin ELISA Crystal Chem USA (Elk Grove Village, IL, USA)
500 according to manufacturer instructions. Blood glucose and insulin levels were
501 integrated into a surrogate measure of whole-body insulin sensitivity using the
502 Matsuda Index:

503 $$Matsuda\ Index = \frac{10{,}000}{\sqrt{(Glucose_0 \times Insulin_0) \times (Glucose_{\mathrm{GTT}\ mean} \times Insulin_{GTT\ mean})}}$$

504

505 *Genetic mapping analysis*

506 Genetic mapping of Matsuda Index was performed in R using the QTL2 package (81)
507 following square root transformation of raw values. The GIGA-MUGA single nucleotide
508 polymorphism array was used as genomic inputs for mapping (79), and a covariate
509 and kinship matrix to account for genetic relatedness amongst the DOz animals.
510 Significance thresholds were established by performing 1000 permutations and set at
511 $P < 0.05$.

512

513 *Caecal DNA isolation*

514 Genomic DNA was extracted from caecal contents of mice using the FastDNA Spin
515 Kit for Feces (MP Biomedicals) as per the manufacturers protocol. DNA concentration
516 was measured using the Qubit dsDNA BR assay kit (Invitrogen). Mock preparations
517 covering all steps of the procedure were conducted as contamination process controls.

518

519 *16S rRNA gene amplicon sequencing analysis*

520 16S rRNA gene amplicon sequencing was performed on all caecal DNA samples.
521 Barcoded amplicon libraries spanning the V4 hypervariable region of the 16S rRNA
522 gene were prepared (515F-806R primer set- 515F: GTGYCAGCMGCCGCGGTAA,
523 806R: GGACTACNVGGGTWTCTAAT) and sequenced using the Illumina MiSeq v2 2
524 x 250 bp platform at the Ramaciotti Centre for Genomics (UNSW, Sydney, Australia).
525 Raw sequence reads were processed using the DADA2 R package which involves
526 using error profiles to define Amplicon Sequence Variants (ASVs)(82). ASVs were
527 assigned to taxonomy using a pre-trained naïve Bayes classifier trained on the curated
528 16S rRNA gene SILVA (v138.1) reference database. Any ASV that was present in
529 fewer than 5% of samples or have less than 0.01% of total reads were filtered from
530 the final dataset prior to downstream analysis. Sequencing depth analyses and
531 rarefaction were performed with the *phyloseq* R package (83).

532 Analysis and graphical presentation of the resultant ASV data was performed in R
533 using the packages *phyloseq*, *vegan*, *microbiome* and *ggplot2*. Alpha diversity metrics
534 were calculated using Inverse Simpson's index, species richness and Shannon's
535 index. Beta diversity was assessed on centred-log-ratio transformed ASV counts using
536 Bray Curtis dissimilarity and UniFrac distance and principal coordinate plots generated
537 from the resultant dissimilarity matrix. PERMANOVA (adonis) using the *vegan* R
538 package was used to assess variance in the distance matrices between groups.
539 Differential abundance analysis was performed using the *ANCOM-BC* R package(84).

540

541 *Intestinal proteomic sample preparation*

542 Division of the small intestine into thirds was achieved by folding the small intestine
543 into three equivalent lengths and taking a 1 cm section of tissue from the centre of

544 each third. These pieces tissue representing the foregut, midgut and hindgut of each
545 mouse were combined and snap frozen in liquid nitrogen. Frozen samples were then
546 boiled in 400 uL of SDC buffer (4% sodium deoxycholate, 100mM Tris-HCl pH 8.0) by
547 heating at 95 C for 10 minutes at 1000 rpm. Samples were then lysed by sonication
548 for 10 minutes (30 seconds on, 30 seconds off, 70% amplitude protocol). Samples
549 were then heated a second time at 95 ºC for 10 minutes at 1,000 rpm before being
550 clarified by centrifugation at 18,000 for 10 minutes at room temperature. Supernatant
551 was taken as lysate and protein concentration was determined by BCA assay, 10 µg
552 of protein was then prepared as previously described (11). Reduction/alkylation
553 (10mM TCEP, 40mM CAA) buffer was added to each sample before incubation for 20
554 minutes at 60 °C. Once cooled to room temperature, 0.4 ug trypsin and 0.4 ug LysC
555 was added to each sample and incubated overnight (18h) at 37 ºC with gentle
556 agitation. 30 µL water and 50 µL 1% TFA in ethyl acetate was added to stop digestion
557 and dissolve any precipitated SDC. Samples were prepared for mass spectrometry
558 analysis by StageTip clean up using SDB-RPS solid phase extraction material
559 (85).(85) Briefly, 2 layers of SDB-RPS material was packed into 200 µL tips and
560 washed by centrifugation at 1,000 x g for 2 minutes with 50 µL acetonitrile followed by
561 0.2% TFA in 30% methanol and then 0.2% TFA in water. 50 µL of samples were
562 loaded to StageTips by centrifugation at 1,000 g for 3 minutes. Stage tips were washed
563 with subsequent spins at 1,000 g for 3 minutes with 50 µL 1% TFA in ethyl acetate,
564 then 1% TFA in isopropanol, and 0.2% TFA in 5% ACN. Samples were eluted by
565 addition of 60µL 60% ACN with 5% NH_4OH_4. Samples were dried by vacuum
566 centrifugation and reconstituted in 30 µL 0.1% TFA in 2% ACN.

567

568 *Mass spectrometry analysis*

569 Peptides prepared as above (2 mg total), were directly injected using a Shimazu LC-
570 40 UHPLC onto a 5 cm x 2.1 mm C18 column analytical column (Agilent InfinityLab
571 Poroshell 120 EC-C18, 1.9 um particles) fitted with a 0.5 cm x 2.1 mm C18 guard
572 column (Agilent InfinityLab Poroshell 120 EC-C18, 1.9 um particles). Peptides were
573 resolved over a gradient from 3% - 36% acetonitrile over 10 min with a flow rate of 0.8
574 mL min^{-1}. Peptide ionization by electrospray occurred at 5.5 kV and a 7600 Zeno TOF
575 mass spectrometer (Sciex) with CID fragmentation used for MS/MS acquisition.
576 Spectra were obtained in a data-independent acquisition using Zeno SWATH with 50
577 isolation width windows spanning 400 to 900 Th. Gas-phase fractionation of a pooled
578 mixture of intestine peptides was performed using 100 Th windows per run, to enable
579 spectral library generation covering the 400-900 Th range. Data files were analyzed
580 using the quantitative DIA proteomics search engine, DIA-NN (version 1.8.1) For
581 spectral library generation, the Uniprot mouse Swissprot database downloaded on the
582 1st of July 2022 was used. Trypsin was set as the protease allowing for 1 missed
583 cleavage and 1 variable modification. Oxidation of methionine were set as a variable
584 modification. Carbamidomethylation of cystine was set as a fixed modification.
585 Remove likely interferences and match between runs were enabled. Neural network
586 classifier was set to double-pass mode. Protein inference was based on genes.
587 Quantification strategy was set to Robust LC (high accuracy). Cross-run normalization
588 was set to RT-dependent. Library profiling was set to full profiling.

589

590 *Peptide synthesis*

591 N,N-dimethylformamide (DMF) and dichloromethane (CH_2Cl_2) for peptide synthesis
592 were purchased from RCI Labscan and Merck. Gradient grade acetonitrile (CH_3CN)
593 for high-performance liquid chromatography was purchased from Sigma Aldrich and
594 ultrapure water (Type 1) was obtained from a Merck Milli-Q EQ 7000 water purification
595 system. Standard Fmoc-protected amino acids (Fmoc-Xaa-OH), coupling reagents
596 and resins were purchased from Mimotopes or Novabiochem. Fmoc-SPPS was
597 performed manually with these reagents and solvents in polypropylene Teflon-fritted
598 syringes purchased from Torviq and through automated synthesis on a SYRO I
599 peptide synthesizer (Biotage). Buffer salts for folding reactions were purchased from
600 Ajax, Sigma Aldrich, and Thermofisher and used as received. Glutathione reduced
601 and oxidised were purchased from Sigma Aldrich and Thermofisher, respectively. All
602 other reagents were purchased from AK Scientific or Merck and used as received.

603 Electrospray mass spectra (ESI-MS) were obtained using a Shimadzu 2020 UPLC-
604 MS with a Nexera X2 LC-30AD pump, Nexera X2 SPD-M30A UV/Vis diode array
605 detector, and a Shimadzu 2020 mass spectrometer using electrospray ionisation (ESI)
606 operating in positive mode. Separations were conducted using a Waters Acquity UPLC
607 BEH300 (1.7 μm, 2.1 x 50 mm C18 column) with a flow rate of 0.6 mL/min. Spectra
608 are recorded from 300-2000 Da.

609 Reverse-phase high performance liquid chromatography (RP-HPLC) was carried out
610 on a Waters 2535 Quaternary Gradient system, fitted with a Waters 2489 UV/Vis
611 Detector (monitoring at 214 and 280 nm) and a Waters Fraction Collector III. Linear
612 peptides were purified by preparative RP-HPLC using an Xbridge C18 column (5 μm,
613 19 × 150 mm) at a flow rate of 12 mL/min. A mobile phase of Milli-Q water (Solvent A)
614 and HPLC-grade CH_3CN (Solvent B) was employed over a linear gradient with 0.1
615 vol% TFA (trifluoroacetic acid) as an additive.

616 Folded peptides were purified by semi-preparative RP-HPLC using a Xbridge C18
617 column (5 µm, 10 × 250 mm) at a flow rate of 4 mL/min. A mobile phase of Milli-Q
618 water (Solvent A) and HPLC-grade CH_3CN (Solvent B) was employed over a linear
619 gradient with 0.1 vol% TFA as an additive.

620 Analytical RP-HPLC was performed on a Waters Alliance e2695 HPLC system
621 equipped with a 2998 PDA detector (λ = 210–400 nm). Separations were performed
622 on a Waters Sunfire® C18 (5 µm, 2.1 × 150 mm) column at 40 ºC with a flow rate of
623 0.5 mL/min. All separations were performed using a mobile phase of 0.1% TFA in
624 water (Solvent A) and 0.1% TFA in CH_3CN (Solvent B) using linear gradients.

625 Peptides were synthesized on a 50 µmol scale. 2-Chlorotrityl chloride (2-CTC) resin
626 was treated with Fmoc-Xaa-OH (1.2 eq) and *i*-Pr_2NEt (4.8 eq) in DCM (4 mL). The C-
627 terminal amino acid of each sequence was used for this loading step, ie. Fmoc-Leu-
628 OH was used for the loading of Def26 and Fmoc-Arg(Pbf)-OH was used for Defa5.
629 Fmoc loading was determined by measuring the piperidine fulvene adduct from Fmoc
630 deprotection. The loading of the resins were: 0.51 mmol/g for Leu on CTC (Def26) and
631 0.50 mmol/g for Arg on CTC (DEFA5).

632

633 <u>General procedure A: Automated Fmoc-Solid-Phase Peptide Synthesis (SPPS) –</u>
634 <u>SYRO I automatic peptide synthesizer (Biotage).</u>

635 50 µmol of the amino acid loaded resin was treated with a solution of piperidine (40
636 vol%, 0.8 mL) in DMF for 3 min, drained, before repeat treatment with piperidine (20
637 vol%, 0.8 mL) in DMF for 10 min. The resin was then drained and washed with DMF
638 (4 x 1.2 mL) before addition of a solution of Fmoc-Xaa-OH (200 µmol, 4 eq.) and
639 Oxyma (4.4 eq.) in DMF (400 µL), followed by a solution of *N,N'*-

640 diisopropylcarbodiimide (4 eq.) in DMF (400 µL). The resin was then agitated at 75 °C
641 for 15 min or 50 °C for 30 min as specified [coupling of Fmoc-His(Trt)-OH and Fmoc-
642 Cys(Trt)-OH were reacted at 50 °C for 30 min in all instances]. The resin was then
643 drained via vacuum and one repeat treatment of the coupling conditions was
644 conducted. The resin was then washed with DMF (4 x 1.2 mL) before being treated
645 with a solution of 5 vol% Ac_2O and 10 vol% *i*-Pr_2NEt in DMF (1.6 mL) and agitated for
646 5 min to cap unreacted N-terminal amines on the growing peptide. The resin was then
647 drained and washed with DMF (4 x 1.6 mL). Iterative cycles of this process were
648 repeated until complete peptide elongation was achieved after which the resin was
649 washed with DMF (4 x 5 mL) and CH_2Cl_2 (5 x 5 mL). HCl counterion exchanges were
650 performed by dissolving the folded peptide in 0.1 M HCl and lyophilising on a freeze
651 drier. This HCl treatment and lyophilisation was repeated 6 times.

652 Synthesis of Def26

653

654 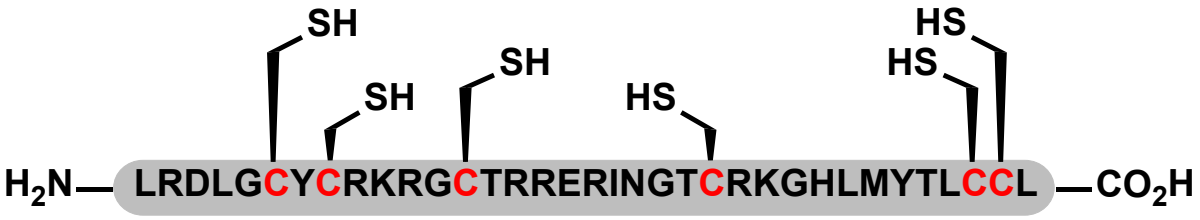

655 Scheme 1. Linear sequence of Def26.

656 The above linear sequence was synthesised according to General Procedure A on 2-
657 CTC resin which was loaded with Fmoc-Leu-OH. The peptide was then cleaved from
658 resin by treatment with 85:5:5:5 v/v/v/v TFA/triisopropylsilane/H_2O/ethanedithiol for 2
659 h at rt. The cleaved solution was collected, dried to ~1 mL under N_2 flow and the
660 peptide product was precipitated using diethyl ether (2 x 40 mL) and collected *via*

661 centrifugation. The crude linear peptide was then purified by preparative RP-HPLC (0
662 vol% CH_3CN + 0.1 vol% TFA for 10 min, then 0-50 vol% CH_3CN + 0.1 vol% TFA over
663 50 min) and lyophilised affording the linear Def26 as a white solid (10.14 mg, 4%).

664 Linear Def26 (5.5 mg, 1 eq) was first dissolved in 220 µL of rapid dilution buffer
665 containing TRIS (50 mM), NaCl (150 mM), guanidine.HCl (6 M), and tris(2-
666 carboxyethyl)phosphine (2 mM). This solution was then added gradually to a buffer
667 containing $NaHCO_3$ (200 mM), urea (2 M), GSH (1 mM), and GSSG (0.2 mM) in MilliQ
668 water to make up a 1 mg/mL peptide solution. The folding reaction was left for 16 h
669 without stirring. The folding progress was monitored through LC-MS, and a loss of 6
670 Da and a simultaneous retention time shift indicated completion of folding. The folded
671 peptide was then purified by semi-preparative RP-HPLC (0 vol% CH_3CN + 0.1% TFA
672 for 20 min, then 0-50 vol% CH_3CN + 0.1 vol% TFA over 50 min), affording the folded
673 Def26 as a white solid after lyophilization (1.07 mg, 19% isolated yield). Prior to
674 biological assays, the peptide was converted to the HCl salt through a HCl counterion
675 exchange.

676 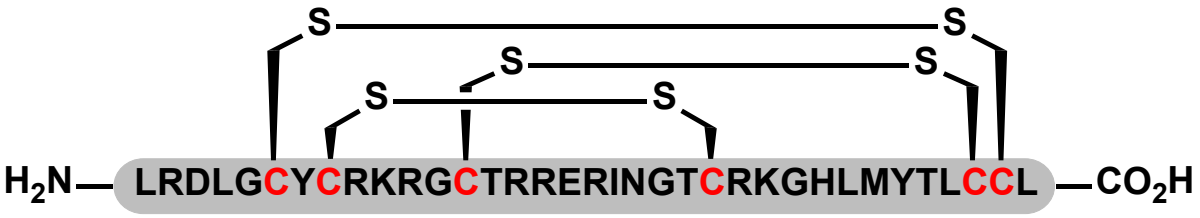

677 Figure S2. Crude semi-preparative scale trace of folded Def26. The first 20 minutes of
678 the 0 vol% B + 0.1 % TFA wash is omitted for clarity. Arrow indicates the collected
679 folded peptide.

680 <u>Synthesis of DEFA5</u>

681 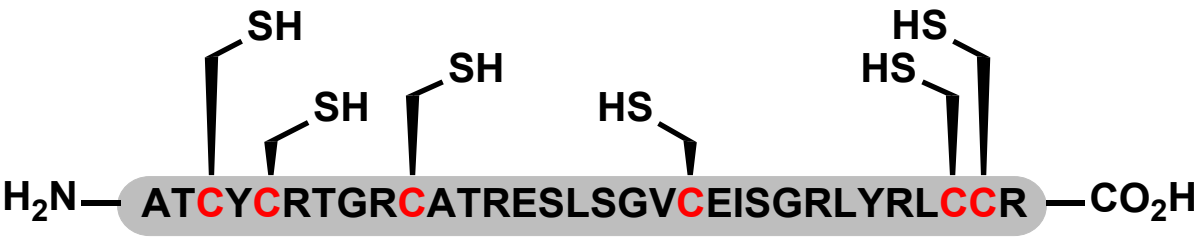

682 Scheme 3. Linear sequence of DEFA5.

683 The above linear sequence was synthesised according to General Procedure A on 2-
684 CTC resin which was loaded with Fmoc-Arg(Pbf)-OH. The peptide was then cleaved
685 from resin by treatment with 85:5:5:5 v/v/v/v TFA/triisopropylsilane/H_2O/ethanedithiol
686 for 2 h at rt. The cleaved solution was collected, dried to ~1 mL under N_2 flow and the
687 peptide product was precipitated using diethyl ether (2 x 40 mL) and collected *via*
688 centrifugation. The crude linear peptide was then purified by preparative RP-HPLC (0
689 vol% CH_3CN + 0.1 vol% TFA for 10 min, then 0-50 vol% CH_3CN + 0.1 vol% TFA over
690 50 min), affording the linear DEFA5 as a white solid after lyophilisation (3.19 mg, 3%).

691 Linear DEFA5 (2.51 mg, 1 eq) was first dissolved in 100 µL of rapid dilution buffer
692 containing TRIS (50 mM), NaCl (150 mM), guanidine.HCl (6 M), and tris(2-
693 carboxyethyl)phosphine (2 mM). This solution was then added gradually to a buffer
694 containing NH_4OAc (330 mM), guanidine.HCl (500 mM), GSH (1 mM), and GSSG (0.2
695 mM) in MilliQ water to make up a 1 mg/mL peptide solution. The folding reaction was
696 then left for 40 h without stirring. The folding progress was determined through LC-
697 MS, and a loss of 6 Da and a simultaneous retention time shift indicated folding. The
698 folded peptide was then purified by semi-preparative RP-HPLC (0 vol% CH_3CN + 0.1%
699 TFA for 20 min, then 0-50 vol% CH_3CN + 0.1 vol% TFA over 50 min), affording the
700 folded DEFA5 as a white solid after lyophilisation (0.62 mg, 24% isolated yield). Prior
701 to biological assays, the peptide was converted to the HCl salt through a HCl
702 counterion exchange.

703

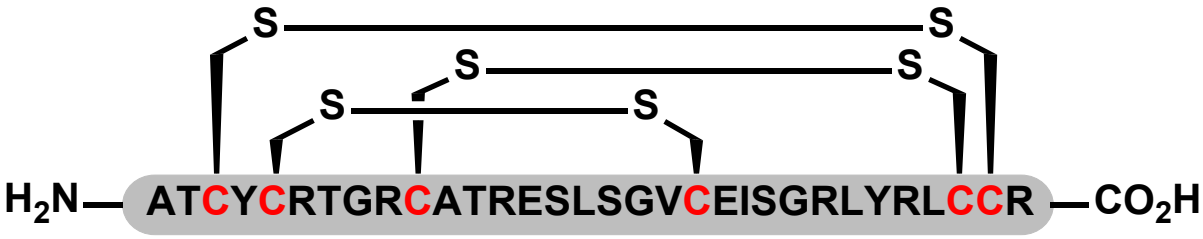

704

705 Scheme 4. Folded sequence of DEFA5.

706

707 *Defensin feeding experiments*

708 Prior to allocation into experimental groups, C57BL/6J and A/J mice underwent
709 baseline metabolic phenotyping was described above. Mice of each strain were then
710 fed a WD or a WD containing the luminal forms of either murine alpha-defensin 26
711 (Def26) or human alpha-defensin 5 (DEFA5) for 8 weeks. Synthetic peptides were
712 mixed into mouse diet by hand. Even distribution of peptides in food was monitored
713 by the addition of blue food dye which was used as a proxy for the distribution of
714 peptides throughout each batch. After eight weeks mice underwent a second bout of
715 metabolic phenotyping and assessment of gut permeability via FITC-dextran oral
716 gavage as previously described (48). Briefly mice were fasted for 4 hours (0900-1300)
717 before a baseline blood sample (50 uL) was taken from a tail incision. Mice were then
718 gavaged with 150 µl of 80 mg/ml FITC dextran (4kDa). After 4 hours, a second blood
719 sample was taken. Both samples (baseline and post-gavage were then centrifuged at
720 5,000 rpm for 10 minutes. Resulting plasma was then diluted 1:10 in PBS and
721 fluorescence was measured at 530 nm with excitation at 485 nm. Data was then
722 expressed as relative fluorescence units.

723

724 *Bile acid extraction*

725 50 µL of plasma thawed on ice was added to 150 µL of ice-cold acetonitrile containing
726 5 pmoles of d4-cholic acid internal standard. Samples were vortexed for 30 s at
727 maximum speed then centrifuged at 15,000 x *g* for 10 min at 4°C to pellet insoluble
728 debris. 170 µL of supernatant was transferred to fused-insert HPLC vials, then vacuum
729 centrifuged to dryness in an Eppendorf Concentrator Plus. Samples were
730 reconstituted in 50 µL of 80:20 water:acetonitrile. All solvents were MS grade.

731

732 *Bile acid quantification*

733 Separation of bile acids was performed using a Nexera LC-40 UHPLC (Shimadzu,
734 Rydalmere NSW) using a 2.1x 50 mm, 2.7 µm CORTECS C18 column (Waters,
735 Rydalmere NSW) with a 7-minute binary gradient of 0.1% formic acid in water (A) and
736 acetonitrile (B) at a flow rate of 0.9 mL/min. Initial gradient conditions of 83:17 A/B rose
737 to 30% B at 1.2 min using curve setting 9. From 1.2 to 3.0 minutes, the proportion of
738 B increased to 38% using curve -5, then rose to 100% at 4.3 min using curve setting
739 5. The column was flushed at 100% B for 1.9 min before returning to initial conditions
740 over 0.1 min and being held for 0.7 min. Column temperature was 50°C and injection
741 volume was 0.5µL.

742 MS data were acquired on a ZenoTOF 7600 (Sciex, Mulgrave VIC) quadrupole-time-
743 of-flight tandem MS operating with electrospray ionisation in negative polarity. Intact
744 bile acid precursor ions were detected using a TOF MS experiment with mass range
745 200-600 Da and accumulation time 0.3 s. Source parameters were: Spray voltage: -
746 4500 V, Temperature: 650°C, Ion source gas 1: 70psi, Ion source gas 2: 80psi, Curtain
747 gas: 40psi. Declustering potential was set to -80 V, collision energy was -10 V and

748 CAD gas was set to 10 (arbitrary units). MS calibration was maintained by Calibrant
749 Delivery System auto-calibration at intervals of approximately 1 hour.

750 Raw data were acquired in a single batch with acquisition order randomised. Six
751 replicates of a sample pool were distributed through the batch to assess intra-batch
752 imprecision. Six replicate injections from a single vial were acquired to determine
753 instrument repeatability. Data analysis was performed with the Analytics module of
754 SCIEX OS (version 3.1.6). Chromatographic peaks were extracted with a width of 0.02
755 Da and integrated using the AutoPeak algorithm. Identification of bile acids was based
756 on both accurate precursor m/z and retention time matched to commercial standards
757 for all quantified bile acid species. Relative molar amounts for bile acids were
758 calculated by comparing raw peak areas relative to the internal standard. Average
759 mass accuracy was >1 ppm, with a range of +/- 2ppm across the run. %CVs were
760 calculated as peak area ratios relative to the internal standard.

Bile Acid	Precursor (Q1) Mass (Da) [M-H]-	Retention Time (min)	Peak Width (min)	%CV Instrument repeatability	%CV Intra-Batch Imprecision
d4 CA	411.3116	2.36	0.15		
CA	407.2803	2.36	0.11	1.17	2.15
DCA	391.2854	3.93	0.19	0.99	6.09
CDCA	391.2854	3.74	0.16	3.63	2.21
UDCA	391.2854	2.45	0.13	5.47	4.9
αMCA	407.2803	1.95	0.08	5.52	12.23
ßMCA	407.2803	2.01	0.09	1.81	2.45
ωMCA	407.2803	1.91 and 2.01	0.08	1.93	2.53
GCA	464.3018	1.94	0.08	1.66	3.25

LCA	375.2905	4.44	0.05	13.49	25.22
TCA	514.2844	1.71	0.10	2.17	5.32
TDCA	498.2895	2.1	0.15	1.99	6.75
TCDCA	498.2895	2.01	0.13	2	5.05
THDCA	498.2895	1.69	0.17	2.29	4.56
TUDCA	498.2895	1.69	0.17	2.29	4.56
TLCA	482.2946	2.88	0.29	1.93	10.3
TßMCA	514.2844	1.53	0.09	2.59	5.47
TωMCA	514.2844	1.5	0.07	3.65	5.89

Data analysis

All data analysis and visualisation were performed in either the R programming environment (86) or GraphPad Prism (GraphPad Software, San Diego, California USA). For protein correlation analysis the Matsuda Index was calculated using glucose tolerance data before being log2 transformed. To correct for multiple testing, p-values were adjusted using the q-value method in the R package *qvalue* (87).(87) Chi-square tests for distribution differences within the data and two/one-way ANOVA tests for group differences were performed in GraphPad Prism.

Acknowledgements

We'd like to thank the Sydney Mass Spectrometry facility and Large Animal Services in the Charles Perkins Centre at the University of Sydney for mass spectrometry and mouse housing support.

Funding

This work was supported by the Australian Research Council (Laureate Fellowship) to David James and by Diabetes Australia (General Grant) to Stewart Masson.

Supplementary Figures

Supplementary Figure 1

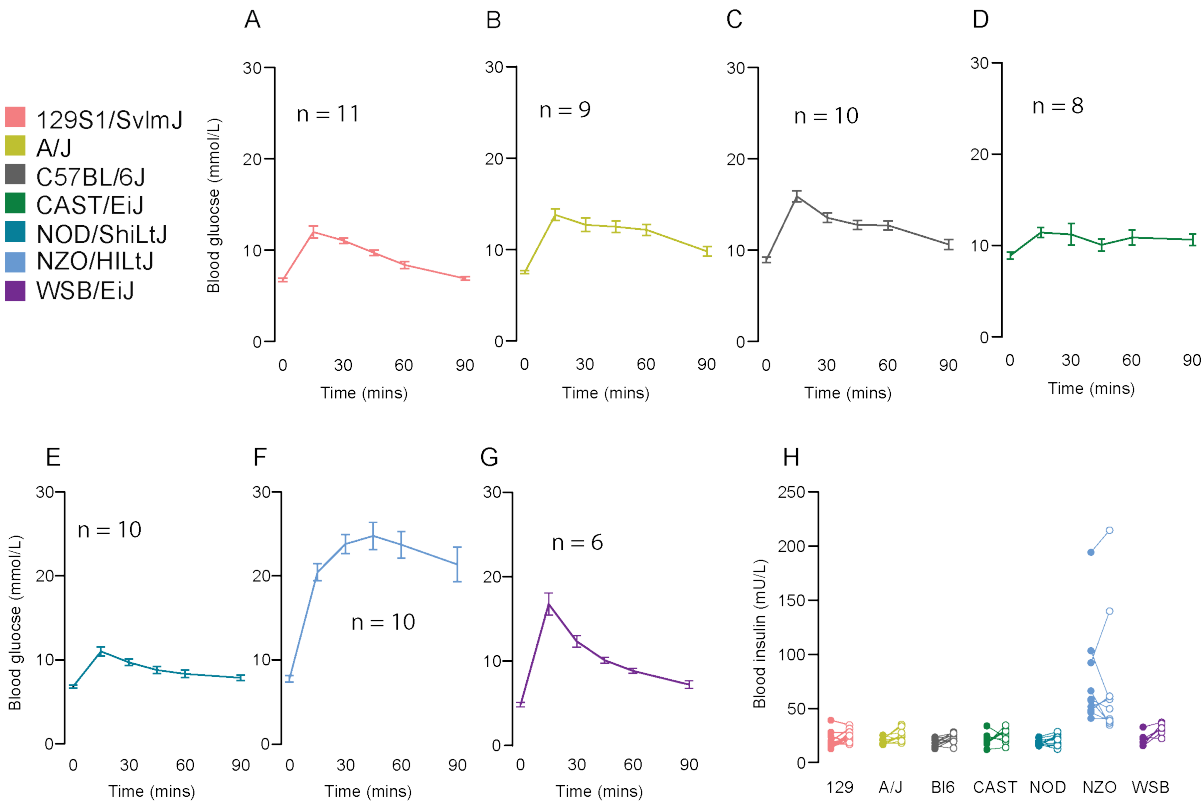

781 **Supplementary Figure 1 – Glucose tolerance and blood insulin concentrations**
782 **in Diversity Outbred founder strains.** Blood glucose concentrations during a
783 glucose tolerance test in **A)** 129S1/SvlmJ, **B)** A/J, **C)** C57BL6/J, **D)** CAST/EiJ, **E)**
784 NOD/ShiLtJ, **F)** NZO/HILtJ, **G)** WSB/EiJ. **H)** Insulin concentration in Diversity Outbred
785 founder strains during a glucose tolerance test. Data are mean with biological
786 replicates are shown as individual data points or noted in figure. **** P < 0.0001, *** P
787 < 0.001, ** P < 0.01, * P < 0.05

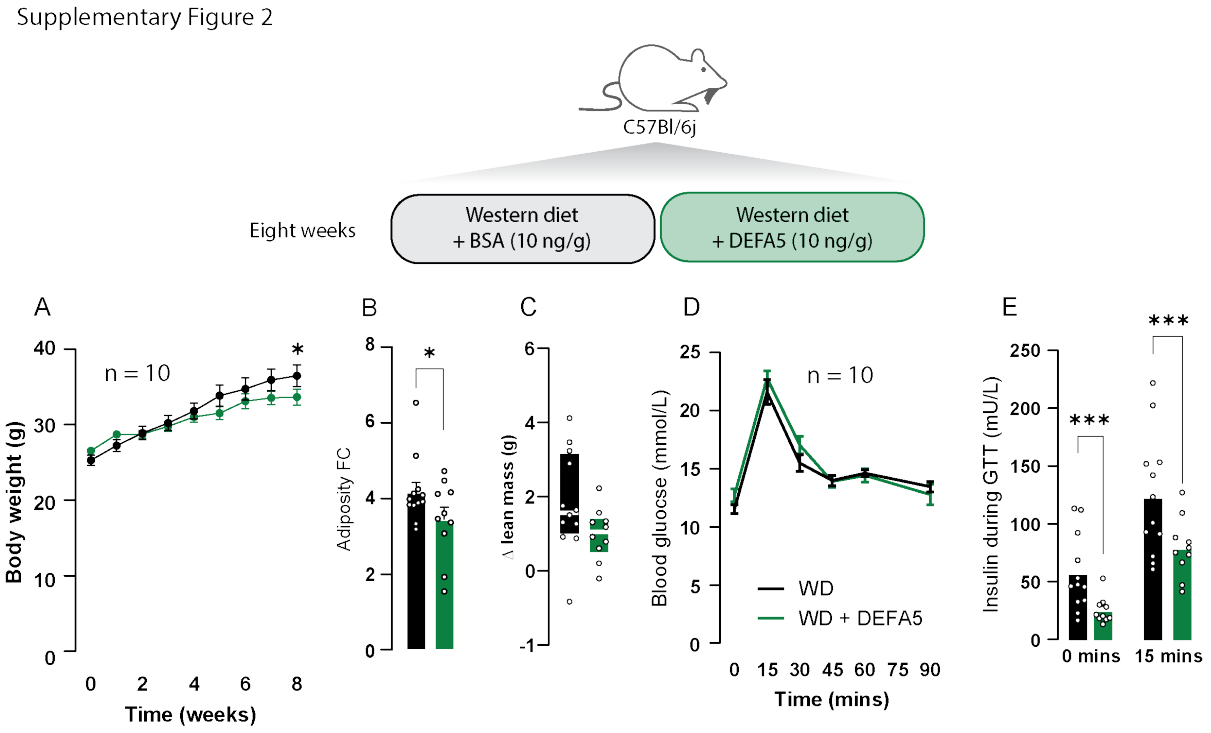

788

789 **Supplementary Figure 2 – Effect of alpha-defensin 5 supplementation on insulin sensitivity and**
790 **body composition in C57BL/6J mice. A)** Body weight of mice fed either WD or WD+DEFA5. **B)** Fold-
791 change in adiposity in mice fed either WD or WD+DEFA5. **C)** Change in lean mass in mice fed either
792 WD or WD+DEFA5. **D)** Blood glucose concentrations in mice fed either WD or WD+DEFA5 during a
793 glucose tolerance test. **E)** Insulin concentrations in mice fed either WD or WD+DEFA5 during a glucose
794 tolerance test. Data are mean with biological replicates are shown as individual data points or in figure.
795 **** P < 0.0001, *** P < 0.001, ** P < 0.01, * P < 0.05

Supplementary Figure 3

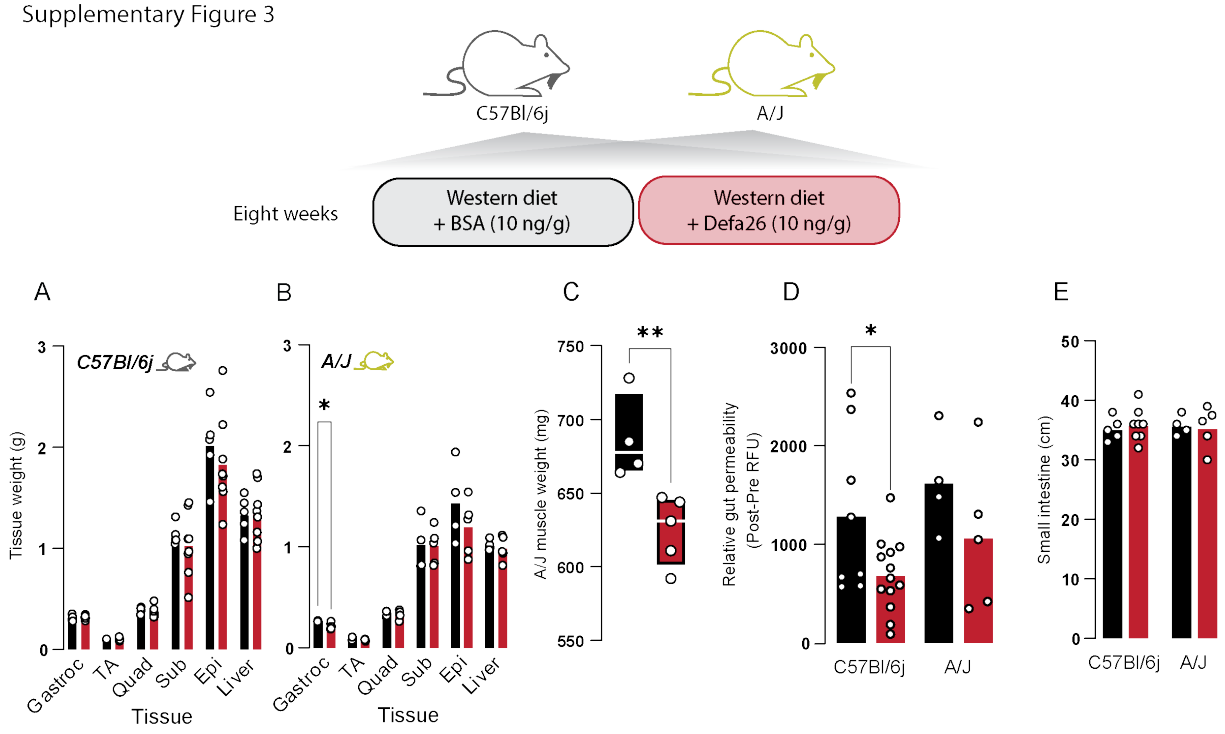

Supplementary Figure 3 – Effect of alpha-defensin 26 supplementation on tissue weights and gut health in C57BL6/J and A/J mice. A) Tissue weights in C57BL/6J mice fed either WD or WD + Def26. **B)** Tissue weights in A/J mice fed either WD or WD + Def26. **C)** Summed muscle (Gastrocnemius, Tibialis anterior, Quadriceps) weights in A/J mice fed either a WD or a WD + Def26. **D)** Relative gut permeability measured by FITC-dextran in C57BL/6J and A/J mice fed either a WD or a WD + Def26. **E)** Small intestine length in C57BL/6J and A/J mice fed either a WD or a WD + Def26. Data are mean with biological replicates are shown as individual data points. **** $P < 0.0001$, *** $P < 0.001$, ** $P < 0.01$, * $P < 0.05$

Supplementary Figure 4

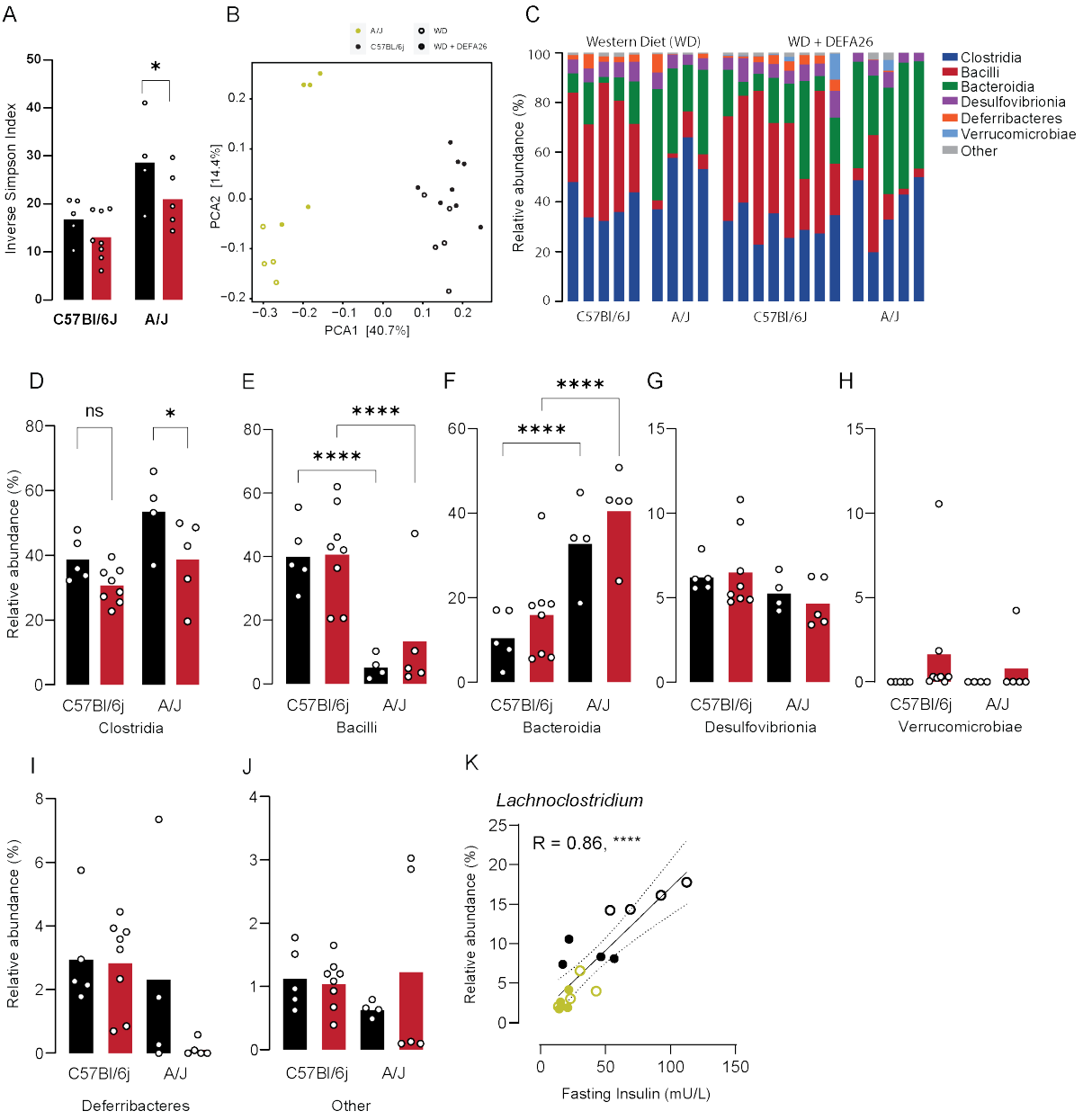

Supplementary Figure 4 – Effect of alpha-defensin 26 (Def26) on microbial composition in western diet (WD)-fed C57BL/6J and A/J mice. A) Alpha-diversity (Inverse Simpson) in WD and WD + Def26 fed C57BL/6J and A/J mice. **B)** Visualisation of beta-diversity (ANCOM-BC) in WD and WD + Def26 fed C57BL/6J and A/J mice. **C)** Relative abundances of microbial taxonomic orders in WD and WD + Def26 fed C57BL/6J and A/J mice. **D)** Relative abundances of Clostrida, **E)** Bacilli, **F)** Bacteriodia, **G)** Desulfovibrionia, **H)** Verrucomicrobiae, **I)** Deferribacteres, **J)** Other taxonomic orders in WD and WD + Def26 fed C57BL/6J and A/J mice. **K)** Correlation of *Lachnoclostridium spp.* with fasting insulin

813 concentrations in WD + Def26 fed C57BL/6J and A/J mice. Data are mean with biological replicates are

814 shown as individual data points. **** $P < 0.0001$, *** $P < 0.001$, ** $P < 0.01$, * $P < 0.05$

Supplementary Figure 5

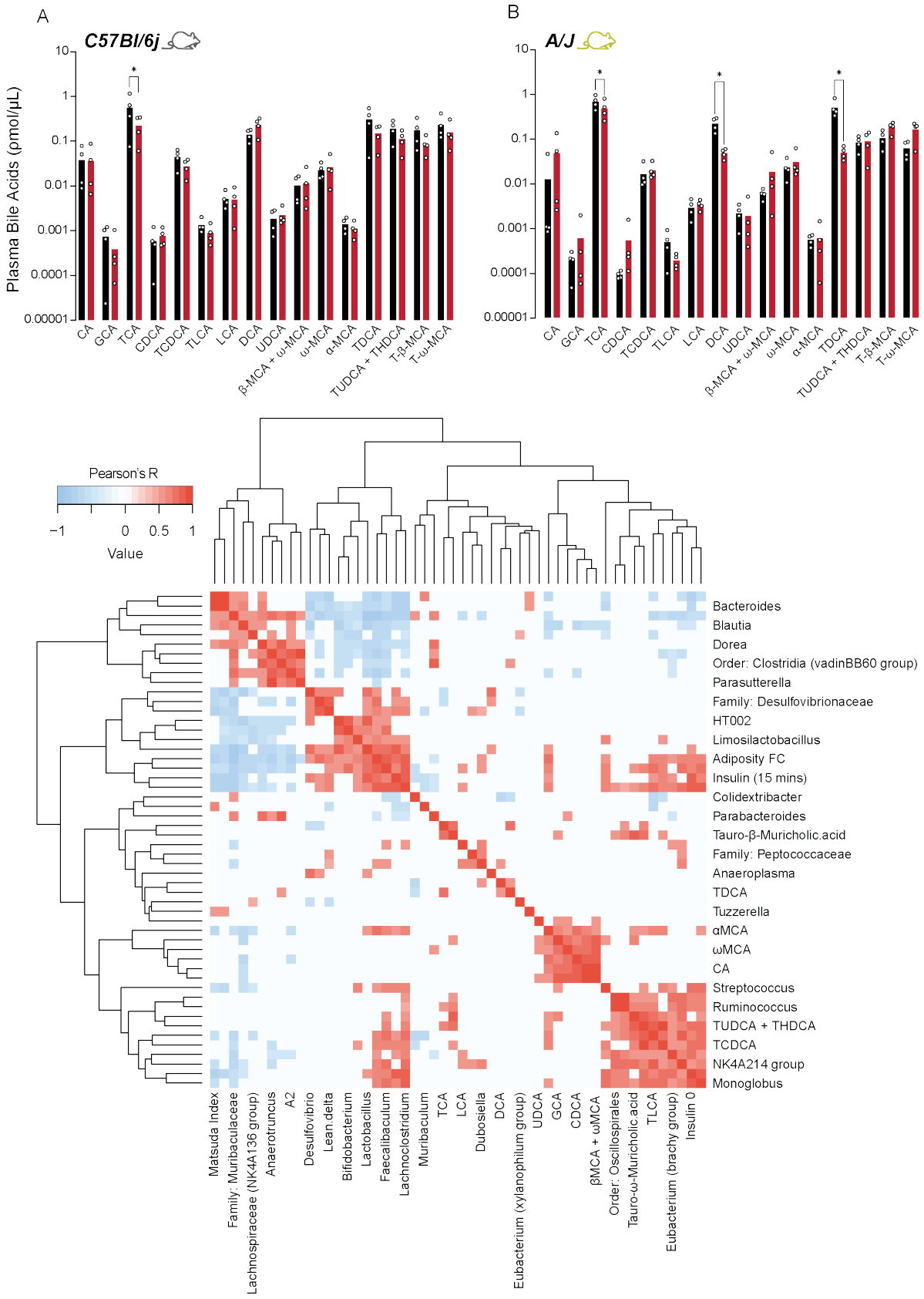

816 **Supplementary Figure 5 – Correlation of plasma bile acid concentrations with metabolically**
817 **microbial genera. A)** Plasma bile acid concentrations in C57BL/6J mice fed either a WD or a WD +
818 Def26. **B)** Plasma bile acid concentrations in A/J mice fed either a WD or a WD + Def26. **C)** Heatmap
819 representation of correlation strength and direction between microbial genera which correlate with
820 metabolic phenotypes and plasma bile acid concentrations. Filled cells represent $p < 0.05$ while colour
821 denotes direction and strength of correlation.

822

823 1. James DE, Stockli J, Birnbaum MJ. The aetiology and molecular landscape of insulin resistance.
824 Nat Rev Mol Cell Biol. 2021;22(11):751-71.
825 2. Diaz-Vegas A, Madsen S, Cooke KC, Carroll L, Khor JXY, Turner N, et al. Mitochondrial electron
826 transport chain, ceramide, and coenzyme Q are linked in a pathway that drives insulin resistance in
827 skeletal muscle. eLife. 2023;12:RP87340.
828 3. Summers SAJPilr. Ceramides in insulin resistance and lipotoxicity. 2006;45(1):42-72.
829 4. Hoehn KL, Salmon AB, Hohnen-Behrens C, Turner N, Hoy AJ, Maghzal GJ, et al. Insulin
830 resistance is a cellular antioxidant defense mechanism. Proc Natl Acad Sci U S A. 2009;106(42):17787-
831 92.
832 5. Fazakerley DJ, Minard AY, Krycer JR, Thomas KC, Stöckli J, Harney DJ, et al. Mitochondrial
833 oxidative stress causes insulin resistance without disrupting oxidative phosphorylation. J Biol Chem.
834 2018;293(19):7315-28.
835 6. D'Souza RF, Masson SWC, Woodhead JST, James SL, MacRae C, Hedges CP, et al. α1-
836 Antitrypsin A treatment attenuates neutrophil elastase accumulation and enhances insulin sensitivity
837 in adipose tissue of mice fed a high-fat diet. Am J Physiol Endocrinol Metab. 2021;321(4):E560-e70.
838 7. Merry TL, Brooks AES, Masson SW, Adams SE, Jaiswal JK, Jamieson SMF, et al. The CSF1
839 receptor inhibitor pexidartinib (PLX3397) reduces tissue macrophage levels without affecting glucose
840 homeostasis in mice. Int J Obes (Lond). 2020;44(1):245-53.
841 8. Scott RA, Lagou V, Welch RP, Wheeler E, Montasser ME, Luan Ja, et al. Large-scale association
842 analyses identify new loci influencing glycemic traits and provide insight into the underlying biological
843 pathways. Nature Genetics. 2012;44(9):991-1005.
844 9. Parks BW, Sallam T, Mehrabian M, Psychogios N, Hui ST, Norheim F, et al. Genetic architecture
845 of insulin resistance in the mouse. Cell Metab. 2015;21(2):334-47.
846 10. Williamson A, Norris DM, Yin X, Broadaway KA, Moxley AH, Vadlamudi S, et al. Genome-wide
847 association study and functional characterization identifies candidate genes for insulin-stimulated
848 glucose uptake. Nature Genetics. 2023;55(6):973-83.
849 11. Nelson ME, Madsen S, Cooke KC, Fritzen AM, Thorius IH, Masson SW, et al. Systems-level
850 analysis of insulin action in mouse strains provides insight into tissue-and pathway-specific
851 interactions that drive insulin resistance. Cell Metabolism. 2022.
852 12. van Gerwen J, Masson SWC, Cutler HB, Vegas AD, Potter M, Stöckli J, et al. The genetic and
853 dietary landscape of the muscle insulin signalling network. Elife. 2024;12.
854 13. Karimkhanloo H, Keenan SN, Bayliss J, De Nardo W, Miotto PM, Devereux CJ, et al. Mouse
855 strain-dependent variation in metabolic associated fatty liver disease (MAFLD): a comprehensive
856 resource tool for pre-clinical studies. Scientific Reports. 2023;13(1):4711.
857 14. Benegiamo G, von Alvensleben GVG, Rodríguez-López S, Goeminne LJE, Bachmann AM, Morel
858 JD, et al. The genetic background shapes the susceptibility to mitochondrial dysfunction and NASH
859 progression. J Exp Med. 2023;220(4).

15. Bachmann AM, Morel JD, El Alam G, Rodríguez-López S, Imamura de Lima T, Goeminne LJE, et al. Genetic background and sex control the outcome of high-fat diet feeding in mice. iScience. 2022;25(6):104468.
16. Churchill GA, Gatti DM, Munger SC, Svenson KL. The Diversity Outbred mouse population. Mamm Genome. 2012;23(9-10):713-8.
17. Chesler EJ, Gatti DM, Morgan AP, Strobel M, Trepanier L, Oberbeck D, et al. Diversity Outbred Mice at 21: Maintaining Allelic Variation in the Face of Selection. G3 (Bethesda). 2016;6(12):3893-902.
18. Gatti DM, Svenson KL, Shabalin A, Wu L-Y, Valdar W, Simecek P, et al. Quantitative Trait Locus Mapping Methods for Diversity Outbred Mice. G3 Genes|Genomes|Genetics. 2014;4(9):1623-33.
19. Svenson KL, Gatti DM, Valdar W, Welsh CE, Cheng R, Chesler EJ, et al. High-resolution genetic mapping using the Mouse Diversity outbred population. Genetics. 2012;190(2):437-47.
20. Masson SWC, Madsen S, Cooke KC, Potter M, Vegas AD, Carroll L, et al. Leveraging genetic diversity to identify small molecules that reverse mouse skeletal muscle insulin resistance. Elife. 2023;12.
21. Thillainadesan S, Lambert A, Cooke KC, Stöckli J, Yau B, Masson SWC, et al. The metabolic consequences of 'yo-yo' dieting are markedly influenced by genetic diversity. Int J Obes (Lond). 2024.
22. Nadeau JH, Auwerx J. The virtuous cycle of human genetics and mouse models in drug discovery. Nature Reviews Drug Discovery. 2019;18(4):255-72.
23. Kau AL, Ahern PP, Griffin NW, Goodman AL, Gordon JI. Human nutrition, the gut microbiome and the immune system. Nature. 2011;474(7351):327-36.
24. Hunt JE, Hartmann B, Schoonjans K, Holst JJ, Kissow H. Dietary Fiber Is Essential to Maintain Intestinal Size, L-Cell Secretion, and Intestinal Integrity in Mice. Front Endocrinol (Lausanne). 2021;12:640602.
25. Berg RD. Bacterial translocation from the gastrointestinal tract. Adv Exp Med Biol. 1999;473:11-30.
26. De Vadder F, Kovatcheva-Datchary P, Zitoun C, Duchampt A, Bäckhed F, Mithieux G. Microbiota-Produced Succinate Improves Glucose Homeostasis via Intestinal Gluconeogenesis. Cell Metab. 2016;24(1):151-7.
27. Canfora EE, Meex RCR, Venema K, Blaak EE. Gut microbial metabolites in obesity, NAFLD and T2DM. Nat Rev Endocrinol. 2019;15(5):261-73.
28. Plovier H, Everard A, Druart C, Depommier C, Van Hul M, Geurts L, et al. A purified membrane protein from Akkermansia muciniphila or the pasteurized bacterium improves metabolism in obese and diabetic mice. Nat Med. 2017;23(1):107-13.
29. Yoon HS, Cho CH, Yun MS, Jang SJ, You HJ, Kim J-h, et al. Akkermansia muciniphila secretes a glucagon-like peptide-1-inducing protein that improves glucose homeostasis and ameliorates metabolic disease in mice. Nature Microbiology. 2021;6(5):563-73.
30. Wahlström A, Sayin SI, Marschall HU, Bäckhed F. Intestinal Crosstalk between Bile Acids and Microbiota and Its Impact on Host Metabolism. Cell Metab. 2016;24(1):41-50.
31. Kreznar JH, Keller MP, Traeger LL, Rabaglia ME, Schueler KL, Stapleton DS, et al. Host Genotype and Gut Microbiome Modulate Insulin Secretion and Diet-Induced Metabolic Phenotypes. Cell Reports. 2017;18(7):1739-50.
32. Qiu Y, Yu J, Li Y, Yang F, Yu H, Xue M, et al. Depletion of gut microbiota induces skeletal muscle atrophy by FXR-FGF15/19 signalling. Ann Med. 2021;53(1):508-22.
33. Zhao L, Yang W, Chen Y, Huang F, Lu L, Lin C, et al. A Clostridia-rich microbiota enhances bile acid excretion in diarrhea-predominant irritable bowel syndrome. The Journal of Clinical Investigation. 2024;130(1):438-50.
34. Lopera-Maya EA, Kurilshikov A, van der Graaf A, Hu S, Andreu-Sánchez S, Chen L, et al. Effect of host genetics on the gut microbiome in 7,738 participants of the Dutch Microbiome Project. Nature Genetics. 2022;54(2):143-51.
35. Goodrich JK, Davenport ER, Beaumont M, Jackson MA, Knight R, Ober C, et al. Genetic Determinants of the Gut Microbiome in UK Twins. Cell Host Microbe. 2016;19(5):731-43.

36. Zhang Q, Linke V, Overmyer KA, Traeger LL, Kasahara K, Miller IJ, et al. Genetic mapping of microbial and host traits reveals production of immunomodulatory lipids by Akkermansia muciniphila in the murine gut. Nat Microbiol. 2023;8(3):424-40.
37. Matsuda M, DeFronzo RA. Insulin sensitivity indices obtained from oral glucose tolerance testing: comparison with the euglycemic insulin clamp. Diabetes Care. 1999;22(9):1462-70.
38. Patil AA, Cai Y, Sang Y, Blecha F, Zhang G. Cross-species analysis of the mammalian beta-defensin gene family: presence of syntenic gene clusters and preferential expression in the male reproductive tract. Physiol Genomics. 2005;23(1):5-17.
39. Nakamura S, Nakamura K, Yokoi Y, Shimizu Y, Ohira S, Hagiwara M, et al. Decreased Paneth cell α-defensins promote fibrosis in a choline-deficient L-amino acid-defined high-fat diet-induced mouse model of nonalcoholic steatohepatitis via disrupting intestinal microbiota. Sci Rep. 2023;13(1):3953.
40. Li J, Li X, Song J, Yan B, Rock SA, Jia J, et al. Absence of neurotensin attenuates intestinal dysbiosis and inflammation by maintaining Mmp7/α-defensin axis in diet-induced obese mice. Faseb j. 2020;34(6):8596-610.
41. Oh YT, Tran D, Buchanan TA, Selsted ME, Youn JH. θ-Defensin RTD-1 improves insulin action and normalizes plasma glucose and FFA levels in diet-induced obese rats. Am J Physiol Endocrinol Metab. 2015;309(2):E154-60.
42. Larsen IS, Fritzen AM, Carl CS, Agerholm M, Damgaard MTF, Holm JB, et al. Human Paneth cell α-defensin-5 treatment reverses dyslipidemia and improves glucoregulatory capacity in diet-induced obese mice. Am J Physiol Endocrinol Metab. 2019;317(1):E42-e52.
43. Ganz T. Defensins: antimicrobial peptides of innate immunity. Nat Rev Immunol. 2003;3(9):710-20.
44. Li Z, Zhang B, Wang N, Zuo Z, Wei H, Zhao F. A novel peptide protects against diet-induced obesity by suppressing appetite and modulating the gut microbiota. Gut. 2023;72(4):686.
45. Depommier C, Everard A, Druart C, Plovier H, Van Hul M, Vieira-Silva S, et al. Supplementation with Akkermansia muciniphila in overweight and obese human volunteers: a proof-of-concept exploratory study. Nat Med. 2019;25(7):1096-103.
46. Gulati AS, Shanahan MT, Arthur JC, Grossniklaus E, von Furstenberg RJ, Kreuk L, et al. Mouse background strain profoundly influences Paneth cell function and intestinal microbial composition. PLoS One. 2012;7(2):e32403.
47. Franck C, Foster SR, Johansen-Leete J, Chowdhury S, Cielesh M, Bhusal RP, et al. Semisynthesis of an evasin from tick saliva reveals a critical role of tyrosine sulfation for chemokine binding and inhibition. Proceedings of the National Academy of Sciences. 2020;117(23):12657-64.
48. Tagesson C, Sjödahl R, Thorén B. Passage of molecules through the wall of the gastrointestinal tract. I. A simple experimental model. Scand J Gastroenterol. 1978;13(5):519-24.
49. Tamai Y, Eguchi A, Shigefuku R, Kitamura H, Tempaku M, Sugimoto R, et al. Association of lithocholic acid with skeletal muscle hypertrophy through TGR5-IGF-1 and skeletal muscle mass in cultured mouse myotubes, chronic liver disease rats and humans. eLife. 2022;11:e80638.
50. Düfer M, Hörth K, Wagner R, Schittenhelm B, Prowald S, Wagner TFJ, et al. Bile Acids Acutely Stimulate Insulin Secretion of Mouse β-Cells via Farnesoid X Receptor Activation and KATP Channel Inhibition. Diabetes. 2012;61(6):1479-89.
51. Krzywinski M, Birol I, Jones SJ, Marra MA. Hive plots--rational approach to visualizing networks. Brief Bioinform. 2012;13(5):627-44.
52. Takeuchi T, Kubota T, Nakanishi Y, Tsugawa H, Suda W, Kwon AT, et al. Gut microbial carbohydrate metabolism contributes to insulin resistance. Nature. 2023;621(7978):389-95.
53. Dabke K, Hendrick G, Devkota S. The gut microbiome and metabolic syndrome. J Clin Invest. 2019;129(10):4050-7.
54. Liu L, Zhang J, Cheng Y, Zhu M, Xiao Z, Ruan G, et al. Gut microbiota: A new target for T2DM prevention and treatment. Front Endocrinol (Lausanne). 2022;13:958218.

55. Hu Y, Flockhart I, Vinayagam A, Bergwitz C, Berger B, Perrimon N, et al. An integrative approach to ortholog prediction for disease-focused and other functional studies. BMC Bioinformatics. 2011;12:357.
56. Costanzo MC, von Grotthuss M, Massung J, Jang D, Caulkins L, Koesterer R, et al. The Type 2 Diabetes Knowledge Portal: An open access genetic resource dedicated to type 2 diabetes and related traits. Cell Metab. 2023;35(4):695-710.e6.
57. Nunn E, Jaiswal N, Gavin M, Uehara K, Stefkovich M, Drareni K, et al. Antibody blockade of activin type II receptors preserves skeletal muscle mass and enhances fat loss during GLP-1 receptor agonism. Mol Metab. 2024;80:101880.
58. Argyrakopoulou G, Gitsi E, Konstantinidou SK, Kokkinos A. The effect of obesity pharmacotherapy on body composition, including muscle mass. Int J Obes (Lond). 2024.
59. Kriaa A, Bourgin M, Potiron A, Mkaouar H, Jablaoui A, Gérard P, et al. Microbial impact on cholesterol and bile acid metabolism: current status and future prospects. J Lipid Res. 2019;60(2):323-32.
60. Pathak P, Xie C, Nichols RG, Ferrell JM, Boehme S, Krausz KW, et al. Intestine farnesoid X receptor agonist and the gut microbiota activate G-protein bile acid receptor-1 signaling to improve metabolism. Hepatology. 2018;68(4):1574-88.
61. Cariou B, van Harmelen K, Duran-Sandoval D, van Dijk TH, Grefhorst A, Abdelkarim M, et al. The farnesoid X receptor modulates adiposity and peripheral insulin sensitivity in mice. J Biol Chem. 2006;281(16):11039-49.
62. Renga B, Mencarelli A, Vavassori P, Brancaleone V, Fiorucci S. The bile acid sensor FXR regulates insulin transcription and secretion. Biochim Biophys Acta. 2010;1802(3):363-72.
63. Zhou W, Akinrotimi O, Dadlani N, Anakk S. FXR Regulates Adipose Tissue Remodeling during Obesity. The FASEB Journal. 2021;35(S1).
64. Correia JC, Massart J, de Boer JF, Porsmyr-Palmertz M, Martínez-Redondo V, Agudelo LZ, et al. Bioenergetic cues shift FXR splicing towards FXRα2 to modulate hepatic lipolysis and fatty acid metabolism. Molecular Metabolism. 2015;4(12):891-902.
65. Sayin SI, Wahlström A, Felin J, Jäntti S, Marschall HU, Bamberg K, et al. Gut microbiota regulates bile acid metabolism by reducing the levels of tauro-beta-muricholic acid, a naturally occurring FXR antagonist. Cell Metab. 2013;17(2):225-35.
66. Orozco-Aguilar J, Tacchi F, Aguirre F, Valero-Breton M, Castro-Sepulveda M, Simon F, et al. Ursodeoxycholic acid induces sarcopenia associated with decreased protein synthesis and autophagic flux. Biological Research. 2023;56(1):28.
67. Mancin L, Wu GD, Paoli A. Gut microbiota-bile acid-skeletal muscle axis. Trends Microbiol. 2023;31(3):254-69.
68. Ueno S, Seino Y, Hidaka S, Nakatani M, Hitachi K, Murao N, et al. Blockade of glucagon increases muscle mass and alters fiber type composition in mice deficient in proglucagon-derived peptides. J Diabetes Investig. 2023;14(9):1045-55.
69. Adeva-Andany MM, Fernández-Fernández C, López-Pereiro Y, Castro-Calvo I, Carneiro-Freire N. The effects of glucagon and the target of rapamycin (TOR) on skeletal muscle protein synthesis and age-dependent sarcopenia in humans. Clinical Nutrition ESPEN. 2021;44:15-25.
70. Fujita S, Rasmussen BB, Cadenas JG, Grady JJ, Volpi E. Effect of insulin on human skeletal muscle protein synthesis is modulated by insulin-induced changes in muscle blood flow and amino acid availability. Am J Physiol Endocrinol Metab. 2006;291(4):E745-54.
71. Samols E, Marri G, Marks V. Interrelationship of glucagon, insulin and glucose. The insulinogenic effect of glucagon. Diabetes. 1966;15(12):855-66.
72. Ishihara H, Maechler P, Gjinovci A, Herrera PL, Wollheim CB. Islet beta-cell secretion determines glucagon release from neighbouring alpha-cells. Nat Cell Biol. 2003;5(4):330-5.
73. Lahiri S, Kim H, Garcia-Perez I, Reza MM, Martin KA, Kundu P, et al. The gut microbiota influences skeletal muscle mass and function in mice. Sci Transl Med. 2019;11(502).

1011 74. Nay K, Jollet M, Goustard B, Baati N, Vernus B, Pontones M, et al. Gut bacteria are critical for
1012 optimal muscle function: a potential link with glucose homeostasis. Am J Physiol Endocrinol Metab.
1013 2019;317(1):E158-e71.
1014 75. Okamoto T, Morino K, Ugi S, Nakagawa F, Lemecha M, Ida S, et al. Microbiome potentiates
1015 endurance exercise through intestinal acetate production. Am J Physiol Endocrinol Metab.
1016 2019;316(5):E956-e66.
1017 76. Safari Z, Bruneau A, Monnoye M, Mariadassou M, Philippe C, Zatloukal K, et al. Murine Genetic
1018 Background Overcomes Gut Microbiota Changes to Explain Metabolic Response to High-Fat Diet.
1019 Nutrients. 2020;12(2).
1020 77. Kootte RS, Levin E, Salojärvi J, Smits LP, Hartstra AV, Udayappan SD, et al. Improvement of
1021 Insulin Sensitivity after Lean Donor Feces in Metabolic Syndrome Is Driven by Baseline Intestinal
1022 Microbiota Composition. Cell Metab. 2017;26(4):611-9.e6.
1023 78. Zhou J, Ho V. Role of Baseline Gut Microbiota on Response to Fiber Intervention in Individuals
1024 with Irritable Bowel Syndrome. Nutrients. 2023;15(22).
1025 79. Morgan AP, Fu CP, Kao CY, Welsh CE, Didion JP, Yadgary L, et al. The Mouse Universal
1026 Genotyping Array: From Substrains to Subspecies. G3 (Bethesda). 2015;6(2):263-79.
1027 80. Broman KW, Gatti DM, Svenson KL, Sen Ś, Churchill GA. Cleaning Genotype Data from Diversity
1028 Outbred Mice. G3 Genes|Genomes|Genetics. 2019;9(5):1571-9.
1029 81. Broman KW, Gatti DM, Simecek P, Furlotte NA, Prins P, Sen Ś, et al. R/qtl2: Software for
1030 Mapping Quantitative Trait Loci with High-Dimensional Data and Multiparent Populations. Genetics.
1031 2019;211(2):495-502.
1032 82. Callahan BJ, McMurdie PJ, Rosen MJ, Han AW, Johnson AJ, Holmes SP. DADA2: High-resolution
1033 sample inference from Illumina amplicon data. Nat Methods. 2016;13(7):581-3.
1034 83. McMurdie PJ, Holmes S. phyloseq: an R package for reproducible interactive analysis and
1035 graphics of microbiome census data. PLoS One. 2013;8(4):e61217.
1036 84. Lin H, Peddada SD. Analysis of compositions of microbiomes with bias correction. Nat
1037 Commun. 2020;11(1):3514.
1038 85. Rappsilber J, Mann M, Ishihama Y. Protocol for micro-purification, enrichment, pre-
1039 fractionation and storage of peptides for proteomics using StageTips. Nat Protoc. 2007;2(8):1896-906.
1040 86. R Core Team R. R: A language and environment for statistical computing. 2013.
1041 87. Dabney A, Storey JD, Warnes GJRpv. qvalue: Q-value estimation for false discovery rate
1042 control. 2010;1(0).

1043